Organic electronic devices and their functional interfaces

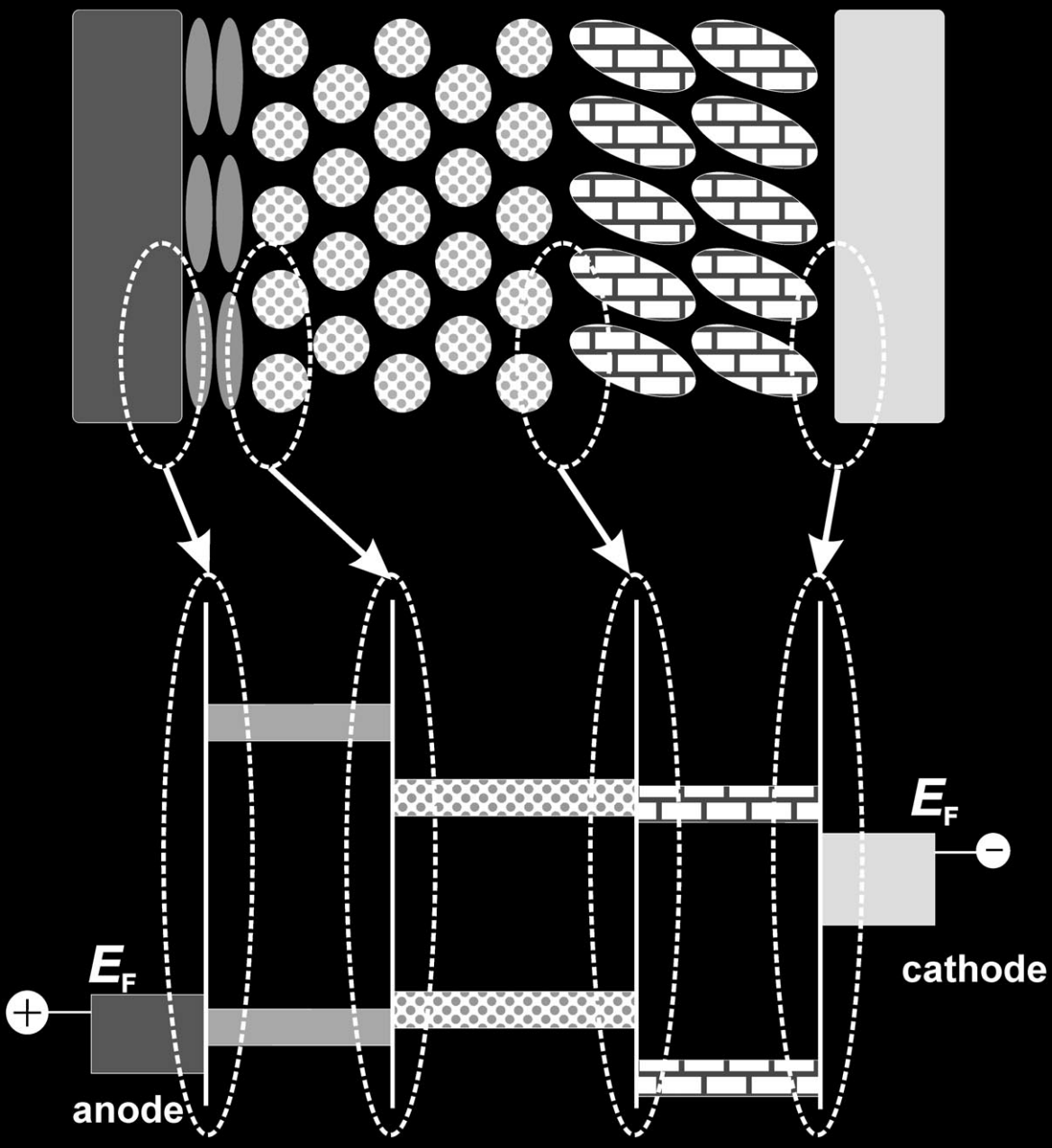

 DOI: 10.1002/cphc.200700177

DOI: 10.1002/cphc.200700177

Organic Electronic Devices and Their Functional Interfaces

Norbert Koch*[a]

A most appealing feature of the development of (opto)electronic devices based on conjugated organic materials is the highly visible link between fundamental research and technological advances. Improved understanding of organic material properties can often instantly be implemented in novel device architectures, which results in rapid progress in the performance and functionality of devices. An essential ingredient for this success is the strong interdisciplinary nature of the field of organic electronics, which brings together experts in chemistry, physics, and engineering, thus softening or even removing traditional boundaries between the disciplines. Naturally, a thorough comprehension of all properties of organic insulators, semiconductors, and conductors is the goal of current efforts. Furthermore, interfaces between dissimilar materials—organic/organic and organic/inorganic—are inherent in organic electronic devices. It has been recognized that these interfaces are a key for device function and efficiency, and detailed investigations of interface physics and chemistry are at the focus of research. Ultimately, a comprehensive understanding of phenomena at interfaces with organic materials will improve the rational design of highly functional organic electronic devices.

1. Introduction

The field of organic electronic devices is characterized by fast-paced progress regarding both efficiency and device function. In addition to the prototypical devices, such as organic light-emitting diodes (OLEDs), thin-film transistors (OTFTs), and photovoltaic cells (OPVCs), further functions have been demonstrated, for example, sensors, memory cells, or light-emitting transistors. As most of these device types can already be realized as "all-organic" (i.e. without inorganic materials), an entirely new technology for an information-based society is envisioned by the integration of the various functional components on one common platform. As a consequence, projections for the potential future market share of organic-based devices are increasing every year. The most intriguing benefits from using organic materials include mechanical flexibility and light weight, which makes this type of device most attractive for mobile applications or "smart clothing". Moreover, entirely new design concepts for consumer electronics have emerged, as organic electronic devices can be adopted to follow complex surface shapes.

The active organic materials are often divided into two classes: small-molecular materials and polymers. While the fundamental properties of both classes are essentially the same, the division mainly relates to the way thin films are prepared. Small molecules are typically thermally evaporated in vacuum and polymers are processed from solution. Yet, most small-molecular materials are soluble as well, or solubility can be increased by the synthetic addition of side chains. A shortcoming of thermal evaporation (sometimes termed "organic molecular-beam deposition"—OMBD) is a rather inefficient use of material, which can be circumvented by using the alternative deposition method of "organic vapor-phase deposition" (OVPD).[1,2] In OVPD, molecules are thermally evaporated into an inert carrier gas stream, which transports the organic material through a heated-wall system to a cool substrate where condensation occurs. Another interesting deposition technique investigated more recently is supersonic molecular-beam deposition (SuMBD), where molecules are accelerated to a few electron volts of kinetic energy by using a seeded supersonic free-jet expansion from a molecular-beam source in which inert gases can be used as a carrier.[3] Controlling the kinetic energy of molecules impinging on the substrate thus provides another parameter to adjust molecular thin-film growth.[3,4] For thin-film preparation from solution, a number of techniques are available in addition to the standard spin-coating method. Of particular interest are inkjet printing, which allows simple direct fabrication of laterally structured circuitry,[5] and various printing techniques[6,7] that enable large-volume roll-to-roll fabrication of organic devices, thus promising comparably low production costs.

Both material classes, polymers and small molecules, have in common the fact that most properties, such as ionization energy, electron affinity, energy gap, solubility, propensity for crystal formation in thin films, and stability in ambient air, can be widely tuned by changing the chemical composition. The large number of already available and newly synthesized materials enable scientists to derive the desired structure–property relationships that are needed for a coherent understanding of conjugated organic materials, and how they can most efficiently be used in optoelectronic devices. Several examples of how

[a] *Dr. N. Koch*
Institut für Physik, Humboldt-Universität zu Berlin
Newtonstr. 15, 12489 Berlin (Germany)
Fax: (+49) 30-2093-7632
E-mail: norbert.koch@physik.hu-berlin.de

better knowledge has helped in providing rational approaches towards device design will be shown in the following. Preference is given to effects that are generally related to interfaces, as these are indeed of paramount importance for device function and performance. Interface energetics and methods to control interface energy-level alignment are discussed in detail in Section 2.1 (in the context of organic light-emitting devices only), but these concepts apply to all subsequent devices alike.

2. Organic Light-Emitting Devices (OLEDs)

The key process for light emission in OLEDs—dc electroluminescence—was reported by Pope et al. in 1963[8] for single crystals of anthracene sandwiched between two electrodes, however, at impractical efficiency. Subsequent research led to the demonstration of comparably efficient OLEDs based on thin films of small molecules by Tang and VanSlyke in 1987,[9] which comprised a double layer of tris(8-hydroxyquinoline)aluminum (Alq_3) as emitter and an aromatic diamine. In 1990, the first polymer-based light-emitting diode (PLED) was introduced by Burroughes et al.,[10] which used poly(*p*-phenylenevinylene). These early reports initiated tremendous research efforts directed towards improving the efficiency and functionality of OLEDs, facilitated by a refined understanding of the individual processes leading to light emission in such devices, some of which can already be derived from the simplest possible OLED energy-level diagram as depicted in Figure 1a. In a single-layer configuration, the active organic layer is sandwiched between a high-work-function (ϕ_1) anode and a low-work-function (ϕ_2) cathode, as used in early device studies. Upon applying an external driving voltage *U*, electrons are injected into the conduction band (CB) and holes into the valence band (VB) of a semiconducting polymer. It should be noted that the concept of electronic bands in polymers is mainly applicable along the direction of an undisturbed polymer chain, as interchain coupling is rather small (i.e. one-dimensional bands). For small-molecular materials, the corresponding energy levels are derived from the lowest unoccupied molecular orbital (LUMO) and the highest occupied molecular orbital (HOMO), which are usually confined to one molecule. Appreciable dispersion of electronic bands relevant for charge transport in molecular materials can only be achieved for highly crystalline defect-free samples.[11–13]

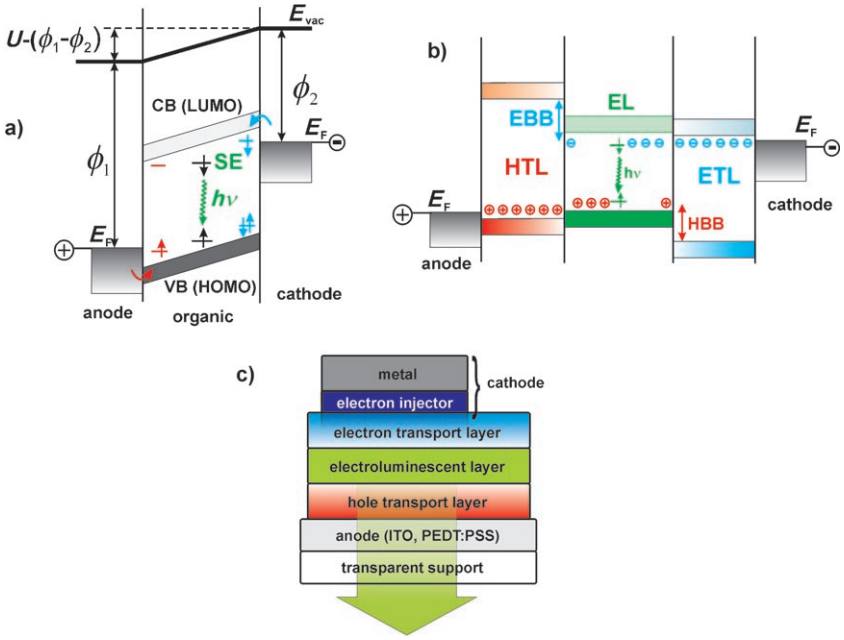

Figure 1. Schematic energy-level diagrams of a) a single-layer OLED and b) a modern multilayer OLED. c) Side view of the layered structure of an OLED. Abbreviations are explained in Section 2.1.6.

Upon injection from the electrodes, electrons and holes self-localize to form negative and positive polarons (indicated in blue and red, respectively, in Figure 1a), which travel under the apparent electric field in opposite directions. When two oppositely charged polarons meet, they can form bound electron–hole pairs (excitons). Exciton formation due to such electrical excitation is governed by spin statistics, which leads to a ratio of 25:75 for singlet excitons (SEs)/triplet excitons (TEs).[14] Note, however, that the issue of singlet/triplet formation ratio is still being debated in the literature,[14–18] and over 50% singlet fractions have been reported.[16–18] In most conjugated organic systems, the lack of heavy atoms in the molecular structure dictates that only SEs can decay radiatively (i.e. produce

Norbert Koch, born in 1971 in Austria, studied physics at the Technische Universität Graz, where he received his diploma (Dipl.-Ing.) and also obtained the doctoral degree (Dr. techn.) in solid-state physics with Günther Leising. After one year as a staff scientist at Joanneum Research GmbH, he joined the groups of Antoine Kahn and Jeffrey Schwartz (Princeton University) as postdoctoral researcher until 2002, and then the group of Jürgen P. Rabe (Humboldt-Universität zu Berlin). Since the end of 2004 he has headed the independent junior research group "Supramolecular Systems" (Emmy Noether Program, DFG) at Humboldt-Universität. His work focuses on the electronic and structural properties of complex functional interfaces with organic materials, and the exploration of new strategies for organic–organic and organic–inorganic heterostructure fabrication.

light), while phosphorescence (see Section 2.2) from longer-lived triplet states is highly improbable. A relation for the quantum efficiency η_Q for OLEDs (number of emitted photons per injected electron) can be derived accordingly [Eq. (1)]:

$$\eta_Q = \gamma \cdot \eta_{ex} \cdot \eta_{pl} \cdot \eta_{oc} \quad (1)$$

where γ is the ratio of injected electrons and holes, η_{ex} the proportion of excitons that can decay radiatively (limited to 25% in systems where phosphorescence does not occur), η_{pl} the efficiency of radiative decay, and η_{oc} the efficiency of light out-coupling (the proportion of photons actually leaving the device). As in display and lighting applications the wavelength-dependent response of the human eye has to be taken into account, the power efficiency η_P ($lm\,W^{-1}$) of OLEDs is proportional to η_Q, the photopic response of the eye, and the ratio of photon energy and device voltage. To maximize efficiency, numerous strategies have been developed to address each of the above contributions, as is detailed below. Consequently, modern OLEDs and PLEDs are multilayer structures (see Figure 1b,c).

2.1. Optimizing the Ratio of Injected Electrons and Holes

There are two physical parameters that influence γ, which ideally should be 1 (i.e. one electron per hole), in order to minimize electrical power losses: i) the injection barrier height and ii) the charge-carrier mobility. As depicted in Figure 1, there are energy barriers for the injection of charges from the electrodes into the charge conduction levels within the organic materials, which correspond to the difference in energy between the electrode Fermi level (E_F) and the organic transport levels at the interface [to first-order approximation within $\approx$0.2 eV below (above) the ground state CB (VB)]. For low operation voltages of OLEDs, these barriers need to be minimized, as the current across such an interface is proportional to the negative exponent of the barrier height in the injection-limited regime.[19]

From the beginning of research in the field of organic electronics onwards, barriers for charge injection at organic/electrode interfaces have commonly been estimated by assuming "vacuum-level alignment" across the interface (i.e. Schottky–Mott limit, as actually shown in Figure 1a) using separately determined values for electrode work function (ϕ) and organic material ionization energy (IE) and electron affinity (EA). Consequently, anode materials should have high ϕ values, and the cathode should have a low ϕ value. Unfortunately, the total neglect of physicochemical phenomena occurring at such interfaces usually results in fairly arbitrary barrier-height values estimated from vacuum-level alignment, except in a few fortunate cases. This was soon realized when experimentally determined hole and electron injection barriers (HIBs, EIBs) were found to be at significant discrepancy (sometimes more than 1 eV) with those estimated using vacuum-level alignment.[20–23] Therefore, significant efforts have been devoted towards developing an understanding of organic/electrode interface energetics and to developing rational methods for controlling (minimizing) injection barriers. Ultraviolet and inverse photoelectron spectroscopy (UPS, IPES) allow the magnitude of HIBs and EIBs, respectively, to be assessed. As UPS probes the occupied levels and IPES the unoccupied ones, both relative to E_F, injection barriers can be directly measured.[22–24] In addition, sample ϕ and the IE of an organic material are obtained from UPS, and EA from IPES.[22–24] One of the most important conclusions from numerous studies was that, by and large, the Schottky–Mott limit does not apply to organic/metal interfaces. Instead, significant changes of ϕ after the deposition of organic molecules were found for clean metal surfaces. The origin of this phenomenon, often termed "vacuum-level shift" or "interface dipole" in the literature, is a rearrangement of the electron density distribution at the metal surface *and* on the molecules due to the mutual interaction at the interface, thus inducing changes of the electrical potential above the surface.

In the case of weak organic–metal interaction (physisorption, which applies to many interfaces between organic materials and clean Au), a qualitative picture of the interface energetics is shown in Figure 2. On the left-hand side, the clean metal surface and the molecule with its LUMO and HOMO levels can be seen at a large distance (no interaction). The metal surface work function has two contributions, namely, the bulk chemical potential μ_{bulk} and the surface dipole (SD), which is due to electrons spilling out into the vacuum at the free surface.[25] Apparently, the HIB could easily be estimated from ϕ and IE assuming vacuum-level alignment. However, we observe that after contact (i.e. molecule adsorption) the work function has been reduced to ϕ', which corresponds to an "interface dipole" (ID), thus leading to a larger HIB than expected. However, this ID does not really exist at the interface, because in fact only the SD of the clean metal surface has been reduced to SD′ due to the "push-back effect" (also known as "cushion effect" or Pauli repulsion in the literature); the adsorption of the organic molecule pushes back the electron density of the metal surface that was spilling out into vacuum. The exact change in total electron density distribution at the organic–metal interface can be rather complex,[26–29] in particular if strong chemical interactions occur,[30,31] and thus depends strongly on the type of molecule and metal.

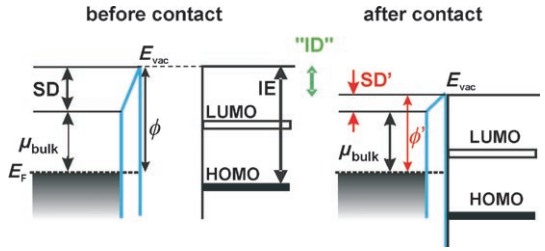

Figure 2. Schematic energy levels at an organic–metal interface with weak interaction (physisorption) "before" and "after" contact, showing that in this case the interface dipole "ID" is a virtual quantity that corresponds to ID = SD − SD′ = $\phi - \phi'$.

2.1.1. Effect of Air Exposure and Residual Contaminants on Organic/Metal Interface Energetics

It is important to emphasize that many studies on organic/metal interfaces were conducted starting from atomically clean metal surfaces in ultrahigh vacuum (UHV; residual pressure $<10^{-9}$ mbar), which is markedly different from the situations that prevail during actual organic device fabrication. In high vacuum (HV; typically 10^{-6} mbar) or inert gas atmospheres, and of course in air, any surface is covered with about a monolayer of various molecular species (e.g. hydrocarbons, oxygen, water) within seconds. As shown above, even physisorbed molecules induce significant changes of ϕ. In addition, some adsorbed species may have permanent dipoles with some preferred orientation relative to the surface, thus leading to additional changes in ϕ ($\Delta\phi$) according to the Helmholtz equation [Eq. (2)]:[32,33]

$$\Delta\phi = \frac{q \cdot N \cdot p}{\varepsilon_0 \cdot \varepsilon_r} \qquad (2)$$

with q the elementary charge, N the surface dipole density, p the dipole moment perpendicular to the surface, ε_0 the vacuum permittivity, and ε_r the relative dielectric constant.

For instance, while an atomically clean Au surface has $\phi \approx 5.1$–5.4 eV in UHV, it drops to ≈ 4.5–4.9 eV after exposure to HV or air, as a rule of thumb[34,35] (the exact value will depend on the composition of the actual atmosphere). Molecules or polymers deposited on such "dirty" Au surfaces exhibit an energy-level alignment that is markedly different from that obtained on clean Au in UHV. Interestingly, due to the fact that most hydrocarbon contaminants from atmospheric air are saturated and often exhibit an ID smaller than that of conjugated molecules, the HIB for subsequently deposited conjugated organic molecules is smaller than that on atomically clean Au by several tenths of an electron volt.[34,35]

Yet another kind of "contamination", however, introduced on purpose in a more controlled way, can significantly lower the HIB at organic/Au interfaces: several minutes of Au surface exposure to UV/ozone. As described in detail elsewhere,[35] this treatment leads to the formation of a thin (ca. monolayer) surface Au-oxide layer, accompanied by the adsorption of oxidized hydrocarbon species. This unique combination leads to an increase of ϕ to up to 5.5 eV (even larger than the ϕ value of clean Au), which is stable in air on the timescale of half an hour. When depositing small-molecular materials or polymers onto UV/ozone-treated Au, the HIBs were reduced by up to 1.4 eV (for blue electroluminescent *p*-sexiphenyl) compared to both atomically clean and air-exposed Au. Furthermore, the energy-level alignment achieved after depositing an organic semiconductor layer was remarkably stable even in air over many days. Contrary to that, an organic/metal interface that was fabricated under UHV conditions changes its energy level alignment upon exposure to air, mainly because oxygen and/or water can diffuse through a thin organic layer towards the metal, and thus modify its electronic properties.[36–38]

2.1.2. Hole Injection Barrier Tuning with Strong Molecular Acceptors

A method that allows continuous adjustment of HIBs at organic/metal interfaces is the precoverage of the metal surface with strong electron-acceptor molecules.[39] The chemisorption of such acceptors is accompanied by an electron transfer from the metal to the molecule, thus introducing local dipoles $\vec{d}$ with their negative ends oriented away from the surface (see Figure 3) and increasing ϕ. The area-averaged work function of a metal surface can thus be adjusted by controlling the area density N of such dipoles. If depolarization effects are small, there exists a linear relationship between the effective ϕ and the molecular coverage from zero to about one monolayer. Subsequently deposited conjugated organic molecules feel this modified average surface potential, and the energy levels are shifted relative to E_F accordingly. For electron acceptors, the occupied levels of virtually any organic material deposited on top of this modified metal surface shift rigidly towards E_F, thus reducing the HIB (right-hand part of Figure 3). Any value for HIB between the two extreme values HIB_{max} (pristine metal surface) and HIB_{min} (ca. monolayer acceptor coverage) can be adjusted predictably by choosing the appropriate acceptor coverage.[39,40]

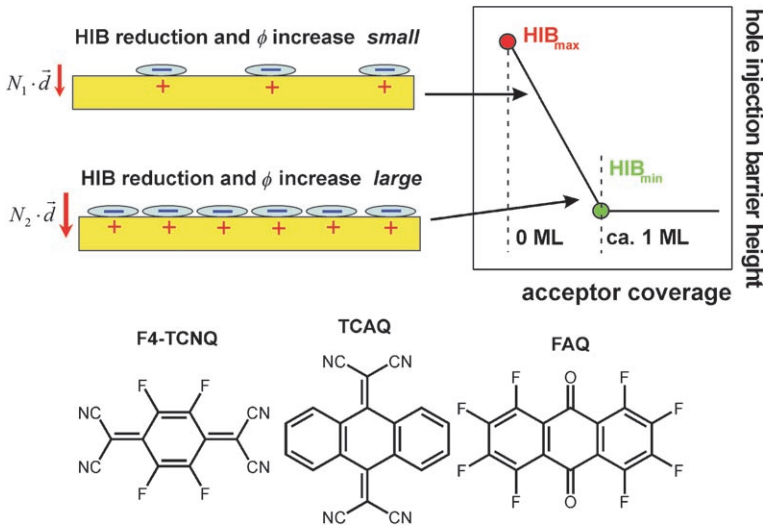

Figure 3. Schematic dependence of the HIB on acceptor-adsorption-induced changes of metal ϕ by local dipoles $\vec{d}$. Bottom: Chemical structures of electron acceptors.

Specific cases that demonstrated the general applicability of this approach to reduce HIBs towards molecular semiconductors include tetrafluorotetracyanoquinodimethane (F4-TCNQ; on Au,[39] Ag, Cu), tetracyanoanthraquinodimethane (TCAQ; on Ag[40]), and octafluoroanthraquinone (FAQ; on Au and Ag[41]). The largest reduction of the HIB achieved with this method so far was 1.2 eV for *p*-sexiphenyl on F4-TCNQ-precovered Au.[39]

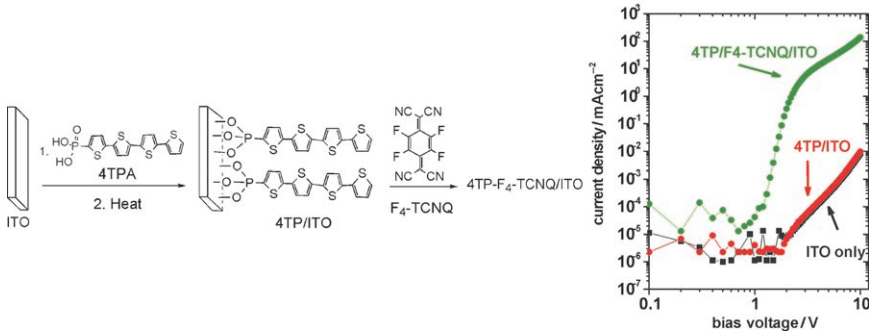

Figure 4. Schematic illustration of the preparation of 4TP/F4-TCNQ on ITO and the effect on hole injection in hole-only devices (single layer of *N*,*N*′-bis(1-naphthyl)-*N*,*N*′-diphenyl-1,1-biphenyl-4,4′-diamine; α-NPD).

2.1.3. Energy-Level Adjustment at Interfaces with Indium Tin Oxide (ITO)

For use in OLEDs, metal surface modification by UV/ozone treatment or molecular acceptors is only relevant for top-emitting devices, where a transparent cathode is deposited on top of the emitting layer.[20,42] More common is the use of an anode consisting of a conducting indium tin oxide (ITO)-covered transparent mechanical support (e.g. glass, plastic), which serves as substrate for subsequently deposited layers. Numerous investigations have been made to elucidate the energetics at interfaces between organic semiconductors and ITO, and how surface treatment of ITO can facilitate low HIBs.[43–52] In fact, both methods presented above, UV/ozone (and oxygen plasma[49,52]) treatment and acceptor adsorption, lead to lowered HIBs for organic materials on ITO. In addition, the use of ITO surface-attached self-assembled monolayers (SAMs) comprising dipolar moieties has been shown to allow adjustment of HIBs towards organic semiconductors, again with the Helmholtz equation as conceptual basis.[53–58] A very successful approach in this direction consists of using phosphonic acid derivatives of fully conjugated moieties, which can self-assemble on ITO to form a dense monolayer. Subsequent annealing leads to the formation of covalent bonds from every molecule to ITO, thus forming a highly stable interface. This has been demonstrated for α-quarterthiophene-2-phosphonic acid (4TPA), which forms a stable covalently bonded monolayer of α-quarterthiophene-2-phosphonate (4TP) on ITO.[59] This SAM can then be rendered highly conductive by immersion in a solution of F4-TCNQ, which forms a charge-transfer complex with the thiophene part of 4TP (as shown schematically in Figure 4). In addition to providing many energy levels close to E_F due to the charge-transfer complex right at the interface, the ϕ of ITO is increased as well, which leads to highly favorable hole injection properties of such an anode (Figure 4). Highly efficient OLEDs with small-molecular materials[59] and polymers[60] were demonstrated using 4TP/F4-TCNQ-modified ITO.

2.1.4. Conducting Polymer Electrodes

Instead of modifying the surface of ITO, the insertion of an intrinsically conducting polymer (ICP) layer between ITO and the luminescent layer has been shown to be very favorable for OLED performance. In addition to doped polyaniline,[61–63] the prototypical ICP used in the majority of applications today is poly(3,4-ethylenedioxythiophene)/poly(styrenesulfonate)[46,64,65] (PEDT:PSS; for chemical structure, see Figure 5), which is used in various formulations. In this polymer mixture, positive charges on the PEDT are stabilized by negative charges on PSS, which renders the conjugated PEDT highly conductive. While PEDT is hydrophobic, PSS is hydrophilic, which results in the formation of small (a few nanometers) core–shell agglomerates in aqueous dispersions, where PSS forms the shell. After spin-coating and drying, highly conductive PEDT-rich domains are separated by insulating PSS-rich domains. Thus, the spatial distribution of alternating volumes of high and low local conductivity can be changed by varying the ratio of PEDT:PSS.[65–69] Through this change of micromorphology it is possible to adjust the overall conductivity of thin films ranging from approximately 10^{-5} S cm^{-1} (1:20) to over 100 S cm^{-1} (1:2.5).[70]

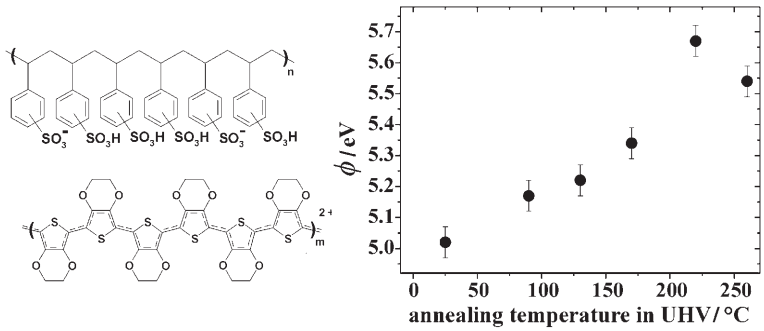

Figure 5. Chemical structure of the conducting polymer mixture PEDT:PSS and the influence of annealing temperature in UHV on its work function ϕ.

While low-conductivity ICPs are mainly used for applications in flat-panel displays (to reduce cross-talk between pixels), the high-conductivity variants allow the inorganic ITO to be completely replaced. The rather complex electronic and morphological properties of ICPs lead to three beneficial effects when used in OLEDs:

1) Application of the ICP layer that is a few tens of nanometers thick significantly flattens the comparably rough surface of ITO, thus providing a smooth surface for the deposition of subsequent layers. This reduces the chance of micro-short formation during operation.
2) High work functions can be achieved for ICPs, which result in low HIBs. (See below for the third effect.)

Some ambiguity exists throughout the organic electronics community regarding the ϕ of PEDT:PSS. Reported values of ϕ vary from approximately 4.8 up to 5.2 eV, and no clear-cut correlations to the formulation or processing conditions used, are made. We recently showed that the ϕ of PEDT:PSS is mainly influenced by residual water in thin films.[71]

As shown in Figure 5, annealing in UHV of PEDT:PSS films spun-cast onto ITO changed ϕ from approximately 5.0 eV (room-temperature drying) to over 5.6 eV (220 °C), which indicates that the intrinsic work function of this ICP can be much higher than that of atomically clean Au. Subsequent exposure of high-ϕ samples to water vapor reduced ϕ to its original value of 5.0 eV. Repeated cycles of annealing/water exposure allowed the reversible change of ϕ within the interval mentioned above. For comparison, PEDT:PSS samples that were annealed in air at 200 °C had a ϕ value of 5.2 eV. Notably, samples that were UHV annealed to exhibit $\phi = 5.6$ eV and then subjected to the simulated atmosphere of a typical inert-gas box (residual water content of ca. 1 ppm H_2O) for 30 min also had a ϕ of 5.2 eV. Furthermore, it was observed that changes in ϕ (and thus water content) were accompanied by changes of the ICP surface composition. While air- and vacuum-annealed sample surfaces were PSS rich, water-vapor-exposed samples had an increased PEDT concentration near the surface. This water-induced swelling can partially account for the observed changes in ϕ, and it was suggested that PSS-surface-rich PEDT:PSS films have a higher ϕ because of preferential orientation of near-surface dipoles (due to the presence of $PEDT^+$ and PSS^-);[72] swelling clearly modified this preferential dipole orientation. Moreover, invoking the Helmholtz equation once more, the inclusion of water in the ICP film may reduce the effect of local dipoles, as the dipole-induced work function changes scale with $1/\varepsilon$, and the dielectric constant ε of water is rather large ($\varepsilon_{H_2O} = 78$). It can be concluded that the residual water content in a PEDT:PSS film has a strong impact on its work function, which can explain the observed variations of ϕ for PEDT:PSS in different laboratories. Finally, it should be noted that ICPs with even higher ϕ are available. These systems comprise additional fluorinated hydrocarbon polymer species, which yield work functions of ≈ 6 eV.[73,74]

In general, this high ϕ of ICPs and the expected small corresponding HIBs towards organic semiconductors has triggered numerous studies on small molecules and polymers alike. It can be stated that low HIBs can indeed be achieved (typically between 0.1 and 0.7 eV, depending on the organic semiconductor). The large number of investigations allows a general picture of the energy-level alignment at interfaces between ICPs and organic semiconductors to be derived. In contrast to metal–organic interfaces, the interface energetics at organic–ICP interfaces seem to follow the Schottky–Mott limit (i.e. vacuum-level alignment) as long as the ϕ of the ICPs falls between an upper ($\phi_{crit\text{-}p}$) and lower ($\phi_{crit\text{-}n}$) critical value. When $\phi_{crit\text{-}p}$ is reached, charge transfer across the interface becomes possible as the Fermi level of the ICP is aligned with the energy position of positive polarons in the organic semiconductor. Further increase of the ICP ϕ leads to the formation of more and more positive polarons at the interface, that is, the energy levels become pinned at this position and an ID is induced by the thermodynamically driven interfacial charge transfer. In analogy, the same phenomenon seems to occur when the ICP ϕ is smaller than $\phi_{crit\text{-}n}$, where the formation of negative polarons in the organic semiconductor becomes feasible and the lowest possible EIB is reached. Furthermore, it has been suggested that the positive (negative) bipolaron levels can also be pinning levels.[75] The transition from the Schottky–Mott limit to energy-level pinning is depicted schematically in Figure 6.

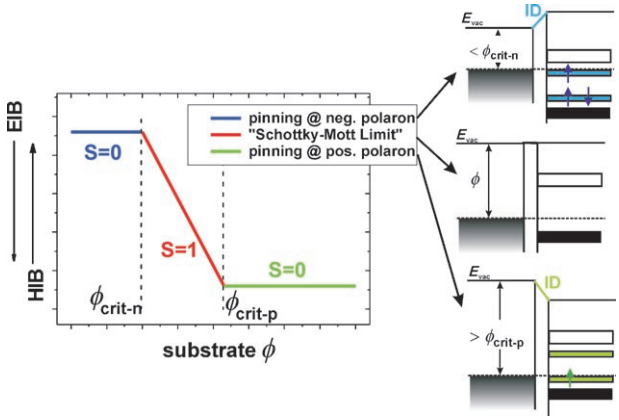

Figure 6. Schematic relationship between the HIB/EIB and work function ϕ of an ICP; HIB and EIB increase in the directions indicated by the arrows on y-axis. Transition from the Schottky–Mott limit ($S = 1$) to energy-level pinning ($S = 0$) at the positive or negative polaron levels of the organic semiconductor. S is a parameter that characterizes the energy-level alignment regime,[23,75] and is defined as $S = dE_F^{gap}/d\phi$, where E_F^{gap} is the position of E_F within the energy gap of the organic semiconductor.

3) The third beneficial effect of PEDT:PSS in OLEDs was recently discussed in several papers: the insulating PSS-rich surface of PEDT:PSS films has electron blocking properties.[76–79]

In most OLEDs based on polymers, that is, PLEDs, the EIB is lower than the HIB (see below), which means that upon application of an increasing driving bias, electrons are injected first. These are transported through the electroluminescent polymer

layer without recombination, as no holes are present. At the interface towards PEDT:PSS the electrons are hindered from entering the ICP layer due to the surface PSS-rich phase, which is insulating (see Figure 7). The accumulation of electrons at

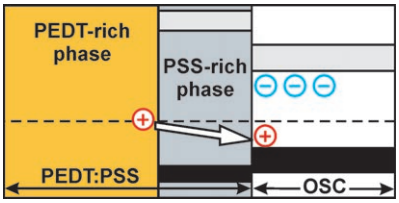

Figure 7. Electron blocking in an organic semiconductor (OSC) at the PSS-rich surface of a PEDT:PSS electrode.

the interface leads to an increase of the local electric field, which facilitates efficient hole injection. Consequently, almost every injected hole can find an electron to form an exciton, which can then recombine. Yet, it remains to be tested whether the proximity of excitons to the highly conductive PEDT:PSS layer could open more nonradiative decay channels.

2.1.5. Low-Work-Function Cathodes

At present, ITO (after various surface treatments) and PEDT:PSS are the most frequently used anode materials in OLEDs. Regarding cathodes, the most straightforward choice would be metals with low work function, for example, Al, Mg (also Mg/Ag mixtures), Ca, and Ba. As these metals are highly reactive, tabulated values for ϕ (usually determined in UHV) can be rather misleading when estimating EIBs. First, these metals can directly react with the organic material, and second, residual oxygen in the vacuum vessel during metal deposition in HV (or subsequent exposure to air) leads to the (partial) formation of metal oxide,[80] whose workfunction can be rather different from that of the pristine metal. For instance, one of the most prominent luminescent and electron-transporting materials, Alq_3, reacts with Al and Mg to form organometallic complexes,[23,81–85] which have new intragap states. Also, many other conjugated materials[86–88] react with Al and Mg, thus leading to a new distribution of occupied and unoccupied levels at such organic–metal interfaces. The description of details of the interaction depends very much on the actual material pairing, and cannot be readily generalized. Furthermore, there are examples where organic materials did not react with Al [*p*-sexiphenyl,[89] methyl-substituted ladder-type poly(*p*-phenylene)[90]] or Mg.[91] However, a more general trend for the interaction with conjugated systems can be stated for alkali and alkaline-earth metals, which are also used to improve electron injection. Quite commonly, the interaction is mainly governed by charge transfer from the metal atoms to the LUMO of the conjugated system, which results in the formation of polarons and/or bipolarons (stabilized by the presence of the metal counterions) that are occupied states within the otherwise empty energy gap.[92–100] The Fermi level becomes pinned at these states, and as they are close in energy to the LUMO of the pristine conjugated system (typically within <0.4 eV) rather low EIBs are the important consequence.

However, since metal cathodes typically are evaporated onto the organic layer, unwanted diffusion of metal atoms into the organic layer has to be prevented (for instance, the presence of metal atoms and ubiquitous chemical reactions with molecules can quench luminescence). Several studies clearly show that metal atoms can diffuse several tens of nanometers into an organic layer.[93,101–103] In this context, the use of alkali halides (e.g. LiF, CsF) has turned out to be very helpful in confining the organic–metal reacted region. A detailed analysis has suggested that alkali halides undergo dissociation when Al is deposited on top, thus releasing the alkali-metal atom to react with the organic semiconductor in immediate proximity.[104–108]

2.1.6. Doped Charge-Transport Layers

We now turn towards another issue of importance for OLED performance. Once the charge carriers have been injected, they need to be transported through the organic layer. Thus, the charge-carrier mobility μ is an important parameter that largely determines at which position from the electrodes exciton formation and recombination can occur, given that HIB and EIB have the same value. Numerous reports conclude that for many conjugated organic materials used in OLEDs, hole mobility (μ_h) is larger than electron mobility (μ_e), often by several orders of magnitude. While the intrinsic physical principle giving rise to this observation is still under debate, low μ_e has often been related to the presence of (oxidative) chemical defects, which act as electron traps.[109–111] As it appears rather difficult to design a material with equal μ_h and μ_e, it seemed plausible to move from single-layer structures (Figure 1 a) to multilayer structures (Figure 1 b,c) in order to confine charge carriers at predetermined positions within the OLED structure, actually very similar to the electron-blocking effect for PEDT:PSS discussed above. As a result, modern OLEDs are multilayer structures, essentially featuring a hole-transport layer (HTL), an electron-transport layer (ETL), and an emission layer (EL) in the middle. The energy levels of materials comprising these three layers must be matched so that an electron-blocking barrier (EBB) exists between the HTL and EL, and a hole-blocking barrier (HBB) between the ETL and EL. Additionally, if the EL is kept rather thin (few tens of nanometers), the probability for electron–hole capture is maximized within the EL layer.

As just mentioned, charge-carrier mobilities are notoriously low in organic materials used in OLEDs, thus resulting in a low conductivity of the individual layers employed, which in turn leads to rather high operation voltages. A huge step towards truly low-operation-voltage devices was made by the introduction of p-doped HTLs and n-doped ETLs, which resulted in p–i–n structures. Doping of organic semiconductors refers to the formation of charge-transfer complexes with strong electron acceptors or donors. P-type doping can be realized efficiently by mixing (e.g. by coevaporation) a few mol% of F4-TCNQ, one of the strongest available molecular electron acceptors, into a matrix of typical hole-transport materials, often aromatic diamines or phthalocyanines.[112–117] When the HOMO

energy of the HTL material matches that of the acceptor, charge transfer can take place, which leads to a new distribution of occupied and unoccupied states close to E_F[114,116–118] thus facilitating high conductivity due to an increase in the number of available charge carriers. N-type doping is frequently realized by the incorporation of alkali-metal atoms, whose ability to donate electrons to organic materials facilitates the formation of polaron/bipolaron states. More recently, organic donor molecules were also used to n-dope electron-transport materials.[119–122] When doped HTLs and ETLs are used, care has to be taken to avoid diffusion of dopant molecules/atoms[116,123] into the EL layer, as luminescence would be quenched by their presence. This can be achieved by either gradually decreasing the dopant concentration towards the EL (as indicated by the fading colors in Figure 1b), or by introducing a thin dopant diffusion-blocking layer at either side of the EL. In addition to providing high conductivity, the presence of the dopants at the same time reduces the HIB and EIB at the anode and cathode, respectively, according to the mechanisms mentioned before (chemisorption of acceptors/donors on inorganic electrode materials involving charge transfer[39]). Even ohmic contacts can be realized.[124]

Using these strategies to reduce injection barriers, increase HTL and ETL conductivity, and provide spatial confinement of the recombination zone results in highly efficienct OLEDs based on small-molecular materials, with low operation voltages and consequently long device lifetimes.[125–127] Matsushima and Adachi[124] realized p–i–n OLEDs (Figure 8) that allowed for

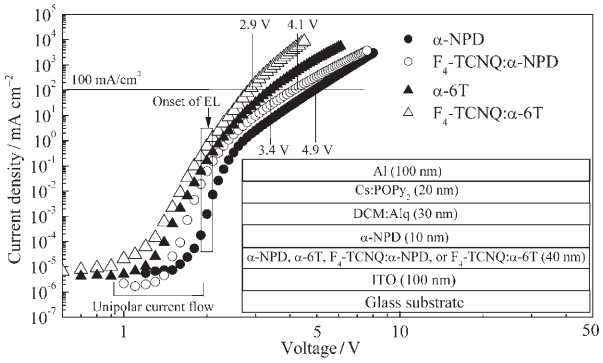

Figure 8. Current–voltage characteristics of a high-performance p–i–n OLED, with the architecture shown in the inset. Cs-doped phenyldipyrenylphosphine oxide ($POPy_2$) as ETL, 4-(dicyanomethylene)-2-methyl-6-(*p*-dimethylaminostyryl) (DCM) mixed into Alq_3 as EL, and F4-TCNQ-doped α-sexithiophene (α-6T) or α-NPD as HTL, with pure α-NPD as acceptor diffusion barrier between HTL and EL. Reprinted with permission from T. Matsushima and C. Adachi, *Appl. Phys. Lett.* **2006**, *89*, 253506.[124] Copyright 2006, American Institute of Physics.

extremely high current density (8.7 A cm^{-2}) and luminance (920000 cd m^{-2}) at low driving voltages (4.5 V), but at moderate power efficiency ($\approx$3 lm W^{-1}). The authors even speculated that this could be a step towards the realization of electrically pumped organic lasers.

2.2. Optimizing the Proportion of Radiatively Decaying Excitons

To circumvent the intrinsic limit of η_{ex} in Equation (1) of 25% for singlet formation in fluorescent materials, the introduction of electrophosphorescent materials by Baldo et al.[128] boosted OLED performance significantly. Phosphorescent emitters are characterized by highly efficient radiative recombination from triplet states $T_1 \rightarrow S_0$ (forbidden for fluorescent emitters), which is facilitated by the presence of heavy atoms in the molecular structure as intercombination transition rates increase due to the heavy-atom effect.[129] For instance, even the presence of heavy atoms due to residual catalysts from polymerization reactions can induce phosphorescence.[130] Typically, a few percent of phosphorescent emitters are mixed (often termed "doped") into a fluorescent host matrix; if the energy levels of the two materials are well chosen, triplets generated by polaron recombination on the host can resonantly transfer to the phosphorescent emitter, thus enabling in principle the realization of $\eta_{ex}=100\%$. In addition, singlets formed on the host material may also be transferred to the phosphorescent emitter, which unfortunately results in a significant energy loss because singlets have to relax via intersystem crossing to the radiative triplet states.[131] Nonetheless, highly efficient OLEDs based on the use of phosphorescent emitters have been realized that cover the entire visible range.

One of the most challenging and also rewarding tasks is the fabrication of white-light-emitting organic devices (WOLEDs) for indoor lighting applications. There is an urgent need for white-light sources with power efficiencies η_P higher than those of inefficient incandescent lamps ($\approx$15 lm W^{-1}).[131,132] In addition to high efficiency and long lifetime, a key requirement for WOLEDs is an emission spectrum that renders white light independent of current density (i.e. overall brightness). Sun et al.[131] recently demonstrated highly efficient ($\eta_P > 23$ lm W^{-1}) WOLEDs with essentially current-density-independent white-light rendition using comparably complex device architectures (Figure 9). The authors propose that 60 lm W^{-1} efficiency should be possible by optimizing their singlet and triplet management strategy.[131] A blue fluorescence emitter and green and red phosphorescence emitters were mixed into a common conductive host [4,4′-bis(*N*-carbazolyl)biphenyl, (CBP)]. However, layers containing the fluorophore were spatially separated from the phosphorescent layers by a few nanometers of undoped CBP (Figure 9a). In addition, a HTL and an ETL were employed. Singlet excitons formed on the host could be transferred via resonant Förster-type transfer to the blue emitter, thus eliminating the energy loss that would occur if a blue phosphorescence emitter was used. Due to the low concentration of fluorescence emitter (5%), host triplets could not efficiently be transferred to it. However, the long diffusion lengths of triplets ($\approx$100 nm)[14] facilitated migration towards the region of green and red phosphors. Consequently, emission from singlets and triplets was achieved through two independent channels, which enable a minimization of energy losses while maximizing the internal quantum efficiency. Most importantly,

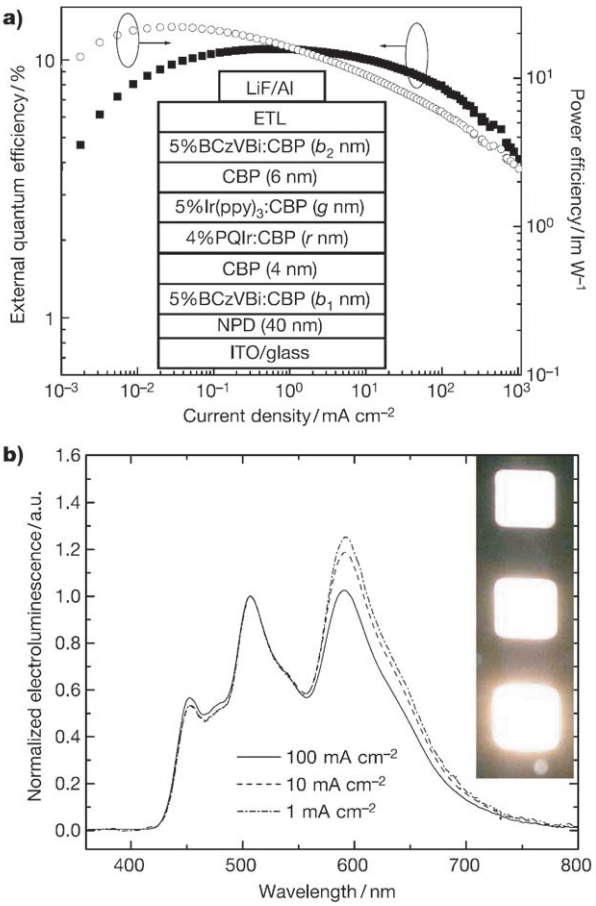

Figure 9. Performance characteristics of a fluorescent/phosphorescent WOLED. a) Forward-viewing external quantum efficiency (■) and power efficiency (○) versus current density of the WOLED structure shown in the inset with layer thicknesses of $b_1 = 15$, $b_2 = 10$, $r = 8$, $g = 12$ nm, and with an ETL consisting of 20 nm 4,7-diphenyl-1,10-phenanthroline (BPhen) followed by 20 nm Li-doped BPhen. b) Normalized electroluminescence spectra of WOLED emission at various current densities. Note that color dependence on current density is minimal. Inset: images of three 4.5 mm^2 devices, each driven at four times the drive current (from 1.7 to 28 mA cm^{-2}) of the device above it in the array to show the color stability of the emission. Reprinted by permission from Macmillan Publishers Ltd.: Nature (Y. Sun, N. C. Giebink, H. Kanno, B. Ma, M. E. Thompson, S. R. Forrest, *Nature* **2006**, *440*, 908[131]), Copyright 2006.

the characteristic white-light emission was essentially independent of driving voltage (Figure 9 b).

While the construction of complex multilayer structures by vacuum sublimation is rather straightforward, controlled multilayer device fabrication with polymer solution processing is inherently more difficult. Quite often, different polymers have similar solubilities in the solvents used, and thus spin-coating a second layer can result in (partial) dissolution of the first layer, which results in unwanted intermixing. Nevertheless, there exist strategies to circumvent this shortcoming. One consists of spin-coating a soluble precursor, which can be converted to the final (insoluble) polymer;[10] another comprises polymerization or crosslinking of reactive side groups, which also render an insoluble polymer layer upon which further layers can be deposited from solution.[133–136] Crosslinking of a spin-coated polymer layer can be achieved by adding an appropriate photoinitiator, which promotes the chemical reaction upon irradiation with light. This can be further exploited for simple structuring of active device areas. This technique was recently applied to fabricate multilayer PLEDs with high efficiency, by using up to two crosslinked hole-transport layers on top of PEDT:PSS (which cannot be dissolved by common organic solvents, as it is based on an aqueous dispersion; see above).[137] For maximizing device efficiency phosphorescence emitters were also employed, which allowed power efficiencies of 10.7 (red emission), 67 (green), and 4.9 lm W^{-1} (blue) to be achieved, clearly demonstrating the huge potential of multilayer PLEDs.

Further research to increase the efficiency of OLEDs is concerned with increasing the luminescence yield of radiative recombination η_{pl}, for example, by spatially separating chromophores that should reduce intermolecular interactions,[138] and by increasing the outcoupling efficiency of light η_{oc}.[139,140]

3. Organic Photovoltaic Cells (OPVCs)

In the 1970s a photovoltaic response in single-layer small-molecule devices was observed,[141,142] and later also for polymer layers,[143] but at very low conversion efficiency. It was soon realized that two dissimilar organic materials need to be combined in order to increase the device performance.[144] Numerous follow-up studies resulted in a fairly good understanding of the interplay of individual processes that lead to the overall function of an OPVC.

According to Figure 10 a, a four-step mechanism leads to the photogeneration and final collection of charges in a simple bilayer device architecture. Two organic semiconductor materials with electron-acceptor (org1) and electron-donor (org2) properties are sandwiched between anode and cathode (typically exhibiting different work functions). In process 1, bound electron–hole pairs (excitons) are generated within one of the organic layers by light absorption. While there is a finite probability for exciton dissociation into a positive and a negative polaron (mobile charge carriers) within one organic layer (mostly at chemical and/or structural defects), this process is significantly more efficient directly at an organic–organic heterojunction with a relative energy-level alignment as shown in Fig-

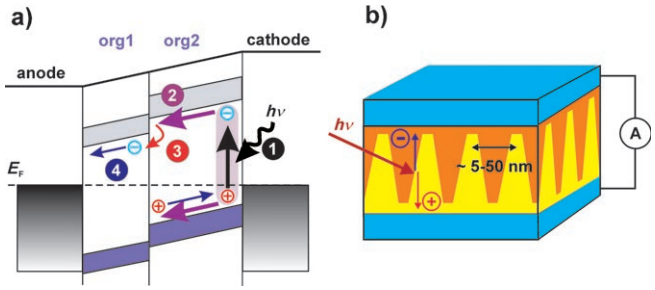

Figure 10. a) Schematic of the four-step operation principle of a bilayer OPVC. b) Model of an optimized OPVC architecture, which comprises maximal organic–organic interface area.

ure 10a. Thus, process 2 is the diffusion of excitons towards the organic–organic interface. Process 3 is the above-mentioned exciton dissociation, which results in electron transfer to the acceptor material and the hole remaining on the donor. Finally, in process 4 the newly generated charge carriers need to be transported towards the respective electrodes. The power conversion efficiency η_P of OPVCs is the ratio of input power (by electromagnetic radiation) and output power (electrical). For a known irradiance E on an active device area A, η_P can be calculated from the maximum current (short-circuit current I_{SC}), maximum voltage (open-circuit voltage V_{OC}), and the fill factor (FF) [Eq. (3)]:

$$\eta_P = \frac{FF \cdot I_{SC} \cdot V_{OC}}{E \cdot A} \quad (3)$$

FF is defined as the maximum power that can be extracted from the actual OPVC divided by the product of I_{SC} and V_{OC}.

From the above-itemized processes, general design principles for the realization of efficient OPVCs can be derived as follows. Regarding process 1, high light absorption coefficients within the organic layers are desirable, ideally covering the entire solar spectrum, which can be well described by the AM 1.5 reference spectrum.[145] Most organic semiconductor absorption spectra cover the energy region above $\approx$1.8 eV fairly well, and efforts are directed towards the synthesis of low-bandgap materials to further include the low-energy part of the solar spectrum[146,147] by alternating donor- and acceptor-moiety copolymers. In general, the absorption coefficients of organic semiconductors are high (on the order of 10^5 cm^{-1}) and almost 100% of the incoming light can be absorbed in films a few hundred nanometers in thickness. However, due to the highly anisotropic electronic properties of many organic semiconductors, the orientation of the relevant transition dipoles with respect to the incoming light has to be considered, in particular in highly ordered organic thin films.[148]

The desired diffusion of excitons towards the organic–organic interface (process 2) poses stringent requirements on the thin-film morphology. Exciton diffusion lengths in polymeric and disordered molecular solids are typically in the range of a few nanometers or a few tens of nanometers, and increase to a few hundred nanometers for highly ordered crystalline samples.[149] Consequently, the average spacing of organic heterojunctions should be on the length scale of the exciton diffusion lengths. This leads to a laterally structured architecture with vertically interdigitated separate phases, as shown schematically in Figure 10b, where every generated exciton should be able to diffuse towards an organic–organic interface. In reality, the fabrication of such ideal structures is inherently difficult with both small-molecular and polymeric materials, in particular because of the small length scales involved. Commonly, so-called bulk heterostructures can be fabricated, where phase separation occurs on the required length scale; however, there are only a few or no continuous percolation paths for charge transport for either electrons or holes within one single phase. Regarding polymer-based OPVCs, an approach consisting of laminating a polymer donor and a polymer acceptor layer allowed a power conversion efficiency of 1.9% to be achieved under a simulated solar spectrum.[150] Subsequent annealing of such structures led to laterally phase-separated areas ($\approx$300 nm) much larger than the exciton diffusion length, which decreased overall efficiency. Mixtures of two polymers,[151,152] a donor polymer and soluble small-molecular acceptor,[153] or two molecular materials from solution[154] resulted in composites of internal donor/acceptor heterojunctions. Due to the limited possibilities of controlling the morphology with high precision when using solution processing, efficiencies were still moderate. Yet, postproduction annealing can have a beneficial influence for the material pair comprising the donor polymer poly(3-hexylthiophene) (P3HT) and the molecular acceptor [6,6]-phenyl-C_{61} butyric acid methyl ester (PCBM). Spin-cast thin films of this mixture were annealed *after* the top Al electrode was evaporated, which led to the formation of a well-defined donor–acceptor interpenetrating network, increased crystallinity of the polymer (resulting in better charge-carrier mobility; see below), and lower electrical resistance at the Al contact, thus resulting in $\eta_P = 5\%$ under AM 1.5 illumination.[155] The importance of a temperature-stable capping layer (e.g. metal or metal oxide) for morphology-preserving post-growth annealing of organic thin films was pointed out earlier by Peumans et al.[156] and Sellner et al.,[157] who showed that using such a layer can effectively suppress substantial surface roughening during annealing or early evaporation of an organic molecular compound. Furthermore, for the prototypical material pair—copper phthalocyanine (CuPc) and 3,4,9,10-perylene tetracarboxylic bis-benzimidazole (PTCBI)—annealing increased the size of bulk heterojunction grains and crystallinity, and such OPVCs exhibited conversion efficiencies of up to 1.4%. As the bulk material probably still contained individual phase grains not connected to the respective electrodes (see Figure 11), further improvements in device efficiency can be expected for better-controlled morphologies.

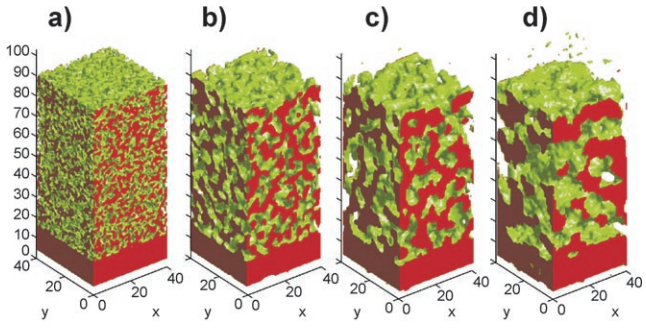

Figure 11. Simulated effects of annealing on the interface morphology of a mixed-layer, small-molecule (copper phthalocyanine, CuPc, and 3,4,9,10-perylene tetracarboxylic bis-benzimidazole, PTCBI) bulk heterojunction photovoltaic cell. a) The initial configuration is generated using a random number generator, and assumes a mixture composition of 1:1. This also assumes that no significant phase segregation occurs during deposition. The interface between CuPc and PTCBI is shown as a green surface. CuPc is shown in red and PTCBI is left "transparent". b–d) The configurations after annealing are shown for increasing annealing temperature. Reprinted by permission from Macmillan Publishers Ltd.: Nature (P. Peumans, S. Uchida, S. R. Forrest, *Nature* **2003**, *425*, 158[156]), Copyright 2003.

A deposition technique that has rarely been applied to organic molecular materials is glancing angle deposition (GLAD), which may prove to be useful to realize ideal OPVC structures as depicted in Figure 10b. In GLAD, a large angle α between the substrate surface normal and the direction of the molecular evaporation source is chosen, while the substrate is rotated about its surface normal during deposition.[158] Due to shadowing effects on lower surface areas during island growth, high-aspect-ratio nanocolumns of organic semiconductor materials can be grown,[159,160] as shown, for instance, in Figure 12 for

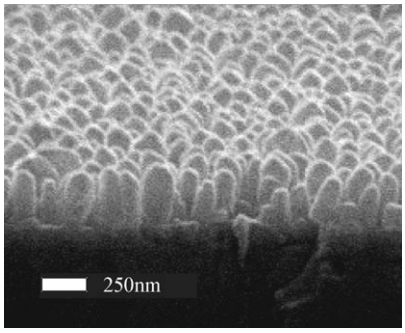

Figure 12. Scanning electron micrograph of a pentacene nanocolumn array on ITO fabricated by GLAD. Image courtesy of Dr. Jian Zhang.

pentacene on ITO. It can be anticipated that by combination with a second organic layer (e.g. prepared via spin-coating) such structures may lead to improved OPVCs.

Process 3 in OPVCs requires that exciton dissociation across the organic–organic interface into free charge carriers is stable, and that recombination of carriers is inhibited. In optimized donor–acceptor material pairs (e.g. polythiophene and C_{60}), charge transfer across the interface happens on a picosecond timescale,[161] thus giving rise to the often-achieved high efficiency of OPVCs fabricated with polythiophene and C_{60} derivatives.[155,162] The most important parameter governing stable charge transfer is the energy-level offset at the organic–organic heterojunction, that is, of "type II", which should exceed several tenths of an electron volt for the valence bands (HOMOs) and conduction bands (LUMOs), respectively. Many organic–organic interfaces seem to follow the simple Schottky–Mott limit at the interface,[163,164] thus enabling the estimation of energy-level diagrams by assuming a common vacuum level. However, there are examples where this model fails,[165–167] and it is still a challenge to derive a coherent understanding of the mechanisms that govern organic–organic interface energetics.[168] Yet another important issue regarding charge separation involves the possible formation of exciplexes (from geminate electron–hole pairs) across the polymer–polymer interface and exciton regeneration, which was deduced from electric-field- and temperature-dependent transient spectroscopy.[169] It was suggested that this effect could be suppressed by a modest increase of intermolecular distances (few nanometers) or reduced electron–phonon coupling of the organic materials.

Finally, process 4 calls for high charge-carrier mobility, to facilitate fast transport of separated charges away from the organic–organic interface and thus minimize exciton regeneration. Charge-carrier mobility is strongly linked to intermolecular order and crystallinity of the organic phases (more details will be discussed in Section 4 on OTFTs). As already mentioned above, postdeposition annealing of organic thin films can significantly increase both crystallinity and the size of crystalline grains; importantly, this can be realized for small-molecular materials and polymer thin films.[156,157,162,170]

4. Organic Thin-Film Transistors (OTFTs)

Thin-film transistors are three-terminal devices, in which the organic semiconductor layer forms the charge-transporting channel between source and drain contacts. In the bottom-contact device configuration (Figure 13a), these contacts are prepat-

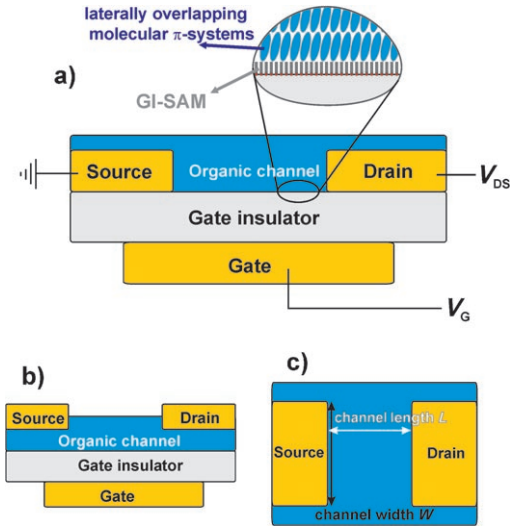

Figure 13. Schematic side view of OTFTs in a) bottom-contact and b) top-contact geometry. c) Top view of OTFT defining channel length *L* and width *W*.

terned on the gate insulator, and the organic material is deposited on top, whereas in the top-contact geometry (Figure 13b) the organic layer is applied to the gate insulator first and the contacts are deposited subsequently (e.g. by evaporation through shadow masks or by soft transfer techniques). In both cases, the gate electrode is capacitively coupled to the channel semiconducting material via the gate insulator. For very pure organic semiconductors, the conductivity within the channel is extremely low because essentially no free charge-carriers are available, and only a very small current would flow at (moderate) voltage between source and drain (V_{DS}). The application of a positive (negative) gate voltage (V_G) gives rise to a large electric field at the organic/insulator interface, which induces negative (positive) charge carriers in its vicinity. These charge carriers can flow in from source and drain contacts when the respective charge-transport levels within the organic channel (adjusted by V_G through the local Fermi level) coincide with the Fermi level of the contacts. This "field effect" renders the channel highly conductive, and results in a significant

source–drain current (I_{DS}). This type of operation is termed enhancement (or accumulation) mode (the device is "off" for $V_G = 0$), while in depletion mode a large current flows for $V_G = 0$ (e.g. for highly doped materials) and I_{DS} can be reduced by the application of a finite gate voltage.[171,172] Most OTFTs work in enhancement mode, and depending on the organic material and device configuration p-channel (hole conducting) or n-channel (electron conducting) behavior can be realized.

To characterize OTFT behavior, a constant V_G can be chosen and I_{DS} measured as a function of V_{DS}. For a set of different V_G values this results in the output characteristics (I_{DS}–V_{DS} curves) exemplified in Figure 14a. Assuming ohmic organic/source and

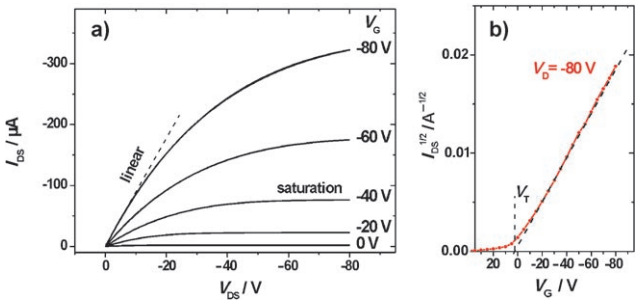

Figure 14. Examples of a) I_{DS}–V_{DS} output characteristics and b) I_{DS}–V_G characteristics of a prototypical OTFT comprising a SiO_2–hexamethyldisilazane (HMDS) gate insulator, Au top contacts, and P3HT as organic semiconductor. The hole mobility extracted from (b) was $\approx 10^{-2}$ cm^2 V s^{-1}. Device data kindly provided by D. Neher and P. Pingel (Universität Potsdam).

-drain contacts,[19] the current can be described in the linear ($I_{DS,lin}$) and saturation ($I_{DS,sat}$) regions by Equations (4) and (5):

$$I_{DS,lin} = \frac{W}{L} C_i \mu (V_G - V_T - V_{DS}/2) V_{DS} \quad (4)$$

$$I_{DS,sat} = \frac{W}{2L} C_i \mu (V_G - V_T)^2 \quad (5)$$

with channel width W, channel length L (see Figure 13c), capacitance per unit area of the gate insulator C_i, the charge-carrier field-effect mobility μ, and the threshold voltage V_T. V_T is a parameter that describes the nonideal behavior of OTFTs, that is, for cases where channel conductance is still considerably large for $V_G = 0$. Depending on the actual device, V_T can be positive or negative, and includes effects related to unwanted doping, deep charge traps, or mismatches of energy levels at the organic/contact interfaces.[173,174] For instance, a positive threshold voltage for p-channel devices may indicate the presence of (unwanted) p-dopants in the organic layer, thus a positive V_G is needed to switch the device off (Figure 14b).

In the linear regime of OTFT operation [Eq. (4)], when $V_{DS} \ll (V_G - V_T)$, the carrier concentration within the channel is essentially independent of the position from source and drain contacts, and I_{DS} is proportional to V_{DS}. Increasing V_{DS} leads to a carrier concentration gradient within the channel (lower concentration near the drain), which leads to a deviation from linear behavior of the output curves. When V_{DS} becomes equal to $(V_G - V_T)$, the gate and the channel region right next to the drain are at the same electrical potential (the channel becomes "pinched"). If V_{DS} is further increased, the region of depletion from free charge carriers near the drain is shifted towards the source,[173] thus implying that I_{DS} does not increase with increasing V_{DS} (saturation regime; Figure 14a). According to Equations (4) and (5), the field-effect mobility can be calculated (e.g. from the slope of a plot $(I_{DS})^{1/2}$ vs V_G; see Figure 14b). However, μ values obtained in the saturation regime are frequently higher than those obtained from the linear regime, because the higher channel resistance in saturation decreases the importance of source/drain contact resistance. In view of the possible applications of OTFTs, the following requirements for device properties can be derived.

At present, high drain currents can only be achieved at rather high V_G and V_{DS} values, typically several tens of volts, which is impractical for mobile applications that require low power consumption. Therefore, high charge-carrier mobility and gate-insulator capacitance are needed. This should be achieved for p-channel *and* n-channel device operation, as both modes of operation are needed for complementary circuit design.

It should be noted that p- and n-channel operation is in principle possible with most organic semiconductor materials. Yet, most presently available materials show exclusively—or at least predominantly—p-type behavior, and significant efforts are made to synthesize materials and fabricate device structures for efficient n-channel OTFTs.[174,175] However, it has been convincingly shown that the limit for good n-channel performance is not necessarily an intrinsic material property; rather it is due to low stability against "doping" in air (by oxygen or reactions with water) and electron trapping at the organic–insulator interface,[176,177] where silanol, carbonyl, or hydroxyl functionalities can have detrimental effects.[176,178] Consequently, finding the right surface termination of the gate insulator is a major issue. The use of SAMs comprising different functional groups and chemical bonding schemes to gate oxides is a common technique, including silane or phosphonate derivatives.[178–181] It should be kept in mind that any surface modification will most likely result in a different organic semiconductor film quality (in terms of crystallinity and density of defects, see below), thus leading to variations of device performance.

While the field-effect mobility achieved occasionally in OTFTs today (over 5 cm^2 V s^{-1} for holes in pentacene[182,183]) is comparable to that of competing amorphous silicon, apparently there is still further potential for even higher mobilities in thin organic films, as work done on structurally perfect single crystals indicates that several tens cm^2 V s^{-1} should be possible. For instance, 35 cm^2 V s^{-1} hole mobility was reported for a pentacene single crystal at room temperature.[184] While carrier mobility generally increases with decreasing temperature in high-quality organic single crystals, indicative of bandlike transport, mobility values increase for elevated temperatures in thin-film samples, where hopping transport prevails.[185] The structural quality of thin films is thus the key for achieving high μ values, as band transport within single grains can be masked by charge-carrier trapping at structural defects, such as disloca-

tions or grain boundaries. In the case of pentacene, the dispersion of the band derived from the HOMO is ≈0.2 eV at room temperature,[13] but grain boundaries significantly reduce the effective mobility observed in thin films. Moreover, the growth and structure of organic films is strongly dependent on the substrate.[186–188] As charge transport in OTFTs is confined to the first few nanometers away from the gate insulator,[189] research has focused on understanding of the growth of the first few monolayers. The electrostatic complexity at the pentacene–silicon oxide interface is a prototypical example[190] (see Figure 15a–c). As can further be seen (Figure 16), standard microscopic techniques may be "blind" to grain boundaries that exist even within apparently isolated single-molecular islands in the submonolayer range. The comparison of a contact-mode atomic force microscopy (AFM) image with the same area scanned in transverse shear mode[190] clearly shows the

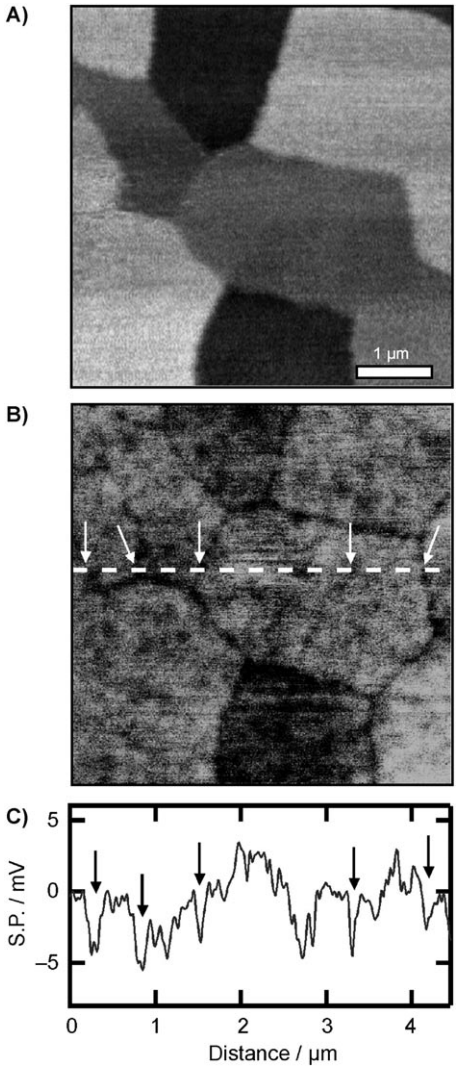

Figure 15. a) Transverse shear and b) surface potential (SP) scanning probe micrographs of a pentacene monolayer on SiO_2, which show potential wells at the grain boundaries. c) SP line section corresponding to the dashed line in (b). The arrows indicate the grain boundary potential wells. The measured depth of the wells averages between ≈−5 and −10 mV over several samples. Reprinted with permission from K. Puntambekar et al.[190]

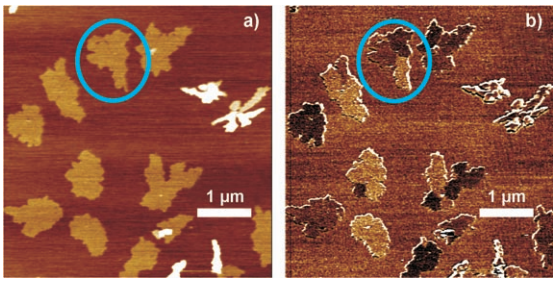

Figure 16. a) Contact mode and b) transverse shear mode AFM images of the same sample area from a pentacene submonolayer on SiO_2. While in contact mode (and tapping mode, not shown) individual islands appear featureless, clear intra-island grain boundaries (e.g. for the island highlighted by a circle, comprising three domains) are observed in (b). Images courtesy of Dr. Jian Zhang.

presence of grain boundaries (where two different color shades within one morphological island in Figure 16b meet) within one island that shows no internal contrast in Figure 16a. Therefore, the area density of grain boundaries in pentacene thin films and individual islands can be significantly underestimated when using simple contact or noncontact AFM imaging modes. It is important to note that pentacene, as an example for many rodlike molecules, can form the well-known layered structures (with almost upright-standing molecules) on rather rough surfaces. Actually, an individual layer can conform very tightly to substrate morphological features, and cover the surface like a "soft carpet". This effect has been observed for substrates such as insulating[191] and conducting polymers.[72] This ability to include vertical offsets between neighboring molecules is exemplified in Figure 17 for a penta-

Figure 17. AFM image of submonolayer pentacene on native silicon oxide with atomic steps. The pentacene islands extend over many steps (step height: 3 Å), as indicated in the schematic side view on the right.

cene submonolayer on native silicon oxide with bunched steps of Si(111) single atomic height (ca. 3 Å). The single-molecule-high islands extend over many substrate steps, and no apparent influence of the substrate morphology can be observed. Such sliding of pentacene neighbors along the long molecular axis can induce traps for electrons and holes on the order of 100 meV.[192] Interestingly, when the height of substrate steps is increased to amount to approximately the molecular length, or when the deposition rate is extremely low, a texture in pentacene islands relative to substrate steps was observed.[193]

For application in radio-frequency identification (RFID) tags, transponders and the load modulator transistors should be compatible with the commercially available base-carrier frequency of 13.56 MHz.[194] Therefore, OTFTs are needed that fully operate in the megahertz regime at reasonable drive voltages. Reduction of the channel length L is a promising strategy for increasing the clock speed, as the cutoff frequency is approximately proportional to $1/L^2$.[19] For example, for a mobility of 0.1 $cm^2 V s^{-1}$, $L < 1$ μm is required to achieve a cutoff frequency of $\approx$10 MHz.[195] Downscaling of the OTFT L to the submicrometer regime can lead to typical short-channel effects,[196] and also the organic–electrode contact resistance, which is in series with the channel resistance, becomes an important parameter. Consequently, strategies to achieve essentially ohmic contacts have to be developed. These efforts can significantly benefit from the work already done within the context of minimizing charge-injection barriers in OLEDs (see Section 2.1). For instance, the use of strong electron-acceptor molecules adsorbed on Au source and drain electrodes,[197] or UV/ozone treatment,[198] could significantly reduce contact resistances in OTFTs.

Recently, novel OTFT structures and architectures were reported, which allow for new device applications and functionality. For instance, organic transistors were fabricated in a cylindrical geometry on a metal–polymer fiber,[199] which represents a significant step towards the full integration of organic electronic devices into "smart clothing". Advanced function was introduced by organic light-emitting transistor (OLET) devices,[200] which combine the switching ability of a transistor and the light emission capability of an OLED; these devices are also under intense investigation at present.[201,202] Very promising for future applications appear to be memory devices based on organic materials. A write-once/read-many-times (WORM) device was realized based on PEDT:PSS,[203] whose conductivity can be strongly reduced by heavy bias-stress. Improved function was introduced by the incorporation of small metal clusters into an organic semiconducting matrix in a two-terminal device,[204,205] which leads to bistable electrical conduction. Switching between high- and low-conductance states is believed to be due to charge transfer to (and storage on) metal clusters within the organic matrix due to energy-level mismatches.[206,207] These devices efficiently function as rewritable nonvolatile memory devices, which are intensively investigated.[207]

5. Conclusions and Outlook

Without doubt, organic electronic devices are an important new technology for applications at various levels. As the fundamental understanding of conjugated organic materials will improve due to the still-growing number of research groups working in this field, the performance of existing devices will be enhanced and novel functional devices will emerge. Interfaces between dissimilar organic and also organic and inorganic materials have been identified as being of particular importance for device function and efficiency. Despite the large number of published investigations, there is still a lack of a truly comprehensive picture of the mechanisms that determine the properties of such interfaces, and how interfaces can predictably be designed and fabricated to satisfy certain requirements. This will require extensive concerted experimental and theoretical efforts, which need to be well designed to allow for clear-cut statements, as presently available theoretical methods have shortcomings regarding an appropriate description of weak interactions and/or very large molecular systems. Theoretical tools that effectively bridge the gap between experiment and modeling are presently being developed.

Key issues of interest for future research include the physicochemical mechanisms that govern the energy-level alignment at organic–electrode and organic–organic interfaces, the conformation of molecules resulting from this interaction, and the dynamics of charge transport and separation at such interfaces. The complex interplay between substrate–molecule and intermolecular interactions during the growth of organic thin films needs to be better understood, to facilitate the realization of desired morphologies and defect-free structures. Moreover, it would be interesting to understand how the chemical structure of molecules must be modified to achieve crystal structures with significant intermolecular interaction, which should boost charge-carrier mobility in organic materials.

Finally, considerable synergies are expected from a strong exchange between researchers working on *organic electronics* and *molecular electronics*. The response of molecules to the presence of interfaces is a common topic in both subject areas. Having rational tools at hand that permit interface properties to be adjusted deliberately over wide ranges will result in advanced organic-based devices that cover macroscopic down to nanoscopic scales.

Acknowledgements

The author would like to thank Prof. Jürgen P. Rabe (HU-Berlin) for stimulating discussions and continued support. Inspiring discussions with Prof. Antoine Kahn and Prof. Jeffrey Schwartz (Princeton University), Dr. Andreas Elschner (H. C. Starck), and Prof. Egbert Zojer and Prof. Emil J. W. List (TU-Graz) are sincerely acknowledged. Furthermore, I would like to thank Patrick Pingel and Prof. Dieter Neher (Universität Potsdam), and Dr. Jian Zhang (HU-Berlin) for providing data. Financial support was provided by the DFG (Sfb448 and Emmy Noether-Program), H. C. Starck GmbH & Co. KG, and the EC (STREP-ICONTOL).

Keywords: electronic devices · electronic structure · interfaces · organic materials · polymers

[1] The term OVPD is a registered trademark of Aixtron AG. For details see https://www.aixtron.com **2007**.
[2] S. R. Forrest, *Chem. Rev.* **1997**, *97*, 1793.
[3] L. Casalis, M. F. Danisman, B. Nickel, G. Bracco, T. Toccoli, S. Iannotta, G. Scoles, *Phys. Rev. Lett.* **2003**, *90*, 206101.
[4] Y. Wu, T. Toccoli, N. Koch, E. Jacob, A. Pallaoro, P. Rudolf, S. Iannotta, *Phys. Rev. Lett.* **2007**, *98*, 076601.
[5] H. Sirringhaus, T. Kawase, R. H. Friend, T. Shimoda, M. Inbasekaran, W. Wu, E. P. Woo, *Science* **2000**, *290*, 2123.

[6] D. A. Pardo, G. E. Jabbour, N. Peyghambarian, *Adv. Mater.* **2000**, *12*, 1249.
[7] T. Mäkelä, S. Jussila, H. Kosonen, T. G. Bäcklund, H. G. O. Sandberg, H. Stubb, *Synth. Met.* **2005**, *153*, 285.
[8] M. Pope, H. Kallmann, P. Magnante, *J. Chem. Phys.* **1963**, *38*, 2042.
[9] C. W. Tang, S. A. VanSlyke, *Appl. Phys. Lett.* **1987**, *51*, 913.
[10] J. H. Burroughes, D. D. C. Bradley, A. R. Brown, R. N. Marks, K. Mackey, R. H. Friend, P. L. Burns, A. B. Holmes, *Nature* **1990**, *347*, 539.
[11] G. N. Gavrila, H. Mendez, T. U. Kampen, D. R. T. Zahn, D. V. Vyalikh, W. Braun, *Appl. Phys. Lett.* **2004**, *85*, 4657.
[12] S. Hasegawa, T. Mori, K. Imaeda, S. Tanaka, Y. Yamashita, H. Inokuchi, H. Fujimoto, K. Seki, N. Ueno, *J. Chem. Phys.* **1994**, *100*, 6969.
[13] N. Koch, A. Vollmer, I. Salzmann, B. Nickel, H. Weiss, J. P. Rabe, *Phys. Rev. Lett.* **2006**, *96*, 156803.
[14] M. A. Baldo, D. F. O'Brien, M. E. Thompson, S. R. Forrest, *Phys. Rev. B* **1999**, *60*, 14422.
[15] M. Reufer, M. J. Walter, P. G. Lagoudakis, B. Hummel, J. S. Kolb, H. G. Roskos, U. Scherf, J. M. Lupton, *Nat. Mater.* **2005**, *4*, 340.
[16] C. Rothe, S. M. King, A. P. Monkman, *Phys. Rev. Lett.* **2006**, *97*, 076602.
[17] J. S. Wilson, A. S. Dhoot, A. J. A. B. Seeley, M. S. Khan, A. Köhler, R. H. Friend, *Nature* **2001**, *413*, 828.
[18] M. Wohlgenannt, K. Tandon, S. Mazumdar, S. Ramasesha, Z. V. Vardeny, *Nature* **2001**, *409*, 494.
[19] S. Z. Sze, *Physics of Semiconductor Devices*, Wiley, New York, **1981**.
[20] H. Ishii, K. Seki, *IEEE Trans. Electron. Devices* **1997**, *44*, 1295.
[21] I. G. Hill, A. Rajagopal, A. Kahn, Y. Hu, *Appl. Phys. Lett.* **1998**, *73*, 662.
[22] H. Ishii, K. Sugiyama, E. Ito, K. Seki, *Adv. Mater.* **1999**, *11*, 605.
[23] A. Kahn, N. Koch, W. Y. Gao, *J. Polym. Sci. Part B* **2003**, *41*, 2529.
[24] D. Cahen, A. Kahn, *Adv. Mater.* **2003**, *15*, 271.
[25] R. Smoluchowski, *Phys. Rev.* **1941**, *60*, 661.
[26] P. S. Bagus, V. Staemmler, C. Wöll, *Phys. Rev. Lett.* **2002**, *89*, 096104.
[27] P. S. Bagus, K. Hermann, C. Wöll, *J. Chem. Phys.* **2005**, *123*, 184109.
[28] G. Witte, S. Lukas, P. S. Bagus, C. Wöll, *Appl. Phys. Lett.* **2005**, *87*, 263502.
[29] N. Koch, A. Vollmer, S. Duhm, Y. Sakamoto, T. Suzuki, *Adv. Mater.* **2007**, *19*, 112.
[30] X. Crispin, C. Bureau, V. M. Geskin, R. Lazzaroni, W. R. Salaneck, J. L. Bredas, *J. Chem. Phys.* **1999**, *111*, 3237.
[31] G. Heimel, L. Romaner, J. L. Bredas, E. Zojer, *Phys. Rev. Lett.* **2006**, *96*, 196806.
[32] G. A. Somorjai, *Introduction to Surface Chemistry and Catalysis*, Wiley, New York, **1994**.
[33] R. Weber, B. Winter, I. V. Hertel, B. Stiller, S. Schrader, L. Brehmer, N. Koch, *J. Phys. Chem. B* **2003**, *107*, 7768.
[34] A. Wan, J. Hwang, F. Amy, A. Kahn, *Org. Electron.* **2005**, *6*, 47.
[35] S. Rentenberger, A. Vollmer, R. Schennach, E. Zojer, N. Koch, *J. Appl. Phys.* **2006**, *100*, 053701.
[36] K. Seki, H. Ishii, *J. Electron Spectrosc. Relat. Phenom.* **1998**, *88*, 821.
[37] C. F. Shen, I. G. Hill, A. Kahn, *Adv. Mater.* **1999**, *11*, 1523.
[38] A. Vollmer, O. D. Jurchescu, I. Arfaoui, I. Salzmann, T. T. M. Palstra, P. Rudolf, J. Niemax, J. Pflaum, J. P. Rabe, N. Koch, *Eur. Phys. J. E* **2005**, *17*, 339.
[39] N. Koch, S. Duhm, J. P. Rabe, A. Vollmer, R. L. Johnson, *Phys. Rev. Lett.* **2005**, *95*, 237601.
[40] N. Koch, S. Duhm, J. P. Rabe, S. Rentenberger, R. L. Johnson, J. Klankermayer, F. Schreiber, *Appl. Phys. Lett.* **2005**, *87*, 101905.
[41] S. Duhm, H. Glowatzki, V. Cimpeanu, J. Klankermayer, J. P. Rabe, R. L. Johnson, N. Koch, *J. Phys. Chem. B* **2006**, *110*, 21069.
[42] G. Parthasarathy, P. E. Burrows, V. Khalfin, V. G. Kozlov, S. R. Forrest, *Appl. Phys. Lett.* **1998**, *72*, 2138.
[43] E. L. Bruner, N. Koch, A. R. Span, S. L. Bernasek, A. Kahn, J. Schwartz, *J. Am. Chem. Soc.* **2002**, *124*, 3192.
[44] C. Ganzorig, K. J. Kwak, K. Yagi, M. Fujihira, *Appl. Phys. Lett.* **2001**, *79*, 272.
[45] I. G. Hill, A. Kahn, *J. Appl. Phys.* **1999**, *86*, 2116.
[46] J. S. Kim, M. Granstrom, R. H. Friend, N. Johansson, W. R. Salaneck, R. Daik, W. J. Feast, F. Cacialli, *J. Appl. Phys.* **1998**, *84*, 6859.
[47] T. Kugler, W. R. Salaneck, H. Rost, A. B. Holmes, *Chem. Phys. Lett.* **1999**, *310*, 391.
[48] Q.-T. Le, E. W. Forsythe, F. Nüesch, L. J. Rothberg, L. Yan, Y. Gao, *Thin Solid Films* **2000**, *363*, 42.
[49] D. J. Milliron, I. G. Hill, C. Shen, A. Kahn, J. Schwartz, *J. Appl. Phys.* **2000**, *87*, 572.
[50] F. Nuesch, E. W. Forsythe, Q. T. Le, Y. Gao, L. J. Rothberg, *J. Appl. Phys.* **2000**, *87*, 7973.
[51] H. Peisert, T. Schwieger, M. Knupfer, M. S. Golden, J. Fink, *J. Appl. Phys.* **2000**, *88*, 1535.
[52] C. C. Wu, C. I. Wu, J. C. Sturm, A. Kahn, *Appl. Phys. Lett.* **1997**, *70*, 1348.
[53] S. F. J. Appleyard, S. R. Day, R. D. Pickford, M. R. Willis, *J. Mater. Chem.* **2000**, *10*, 169.
[54] I. H. Campbell, J. D. Kress, R. L. Martin, D. L. Smith, N. N. Barashkov, J. P. Ferraris, *Appl. Phys. Lett.* **1997**, *71*, 3528.
[55] R. A. Hatton, S. R. Day, M. A. Chesters, M. R. Willis, *Thin Solid Films* **2001**, *394*, 292.
[56] P. K. H. Ho, M. Granstrom, R. H. Friend, N. C. Greenham, *Adv. Mater.* **1998**, *10*, 769.
[57] H. Yan, Q. L. Huang, J. Cui, J. G. C. Veinot, M. M. Kern, T. J. Marks, *Adv. Mater.* **2003**, *15*, 835.
[58] L. Zuppriolli, L. Si-Ahmed, K. Kamaras, F. Nüesch, M. N. Bussac, D. Ades, A. Siove, E. Moons, M. Grätzl, *Eur. Phys. J. B* **1999**, *11*, 505.
[59] E. Hanson, J. Guo, N. Koch, J. Schwartz, S. L. Bernasek, *J. Am. Chem. Soc.* **2005**, *127*, 10058.
[60] J. Guo, N. Koch, S. L. Bernasek, J. Schwartz, *Chem. Phys. Lett.* **2006**, *426*, 370.
[61] L. T. Hou, Q. Hou, Y. Q. Mo, J. B. Peng, Y. Cao, *Appl. Phys. Lett.* **2005**, *87*, 243504.
[62] J. C. Scott, S. A. Carter, S. Karg, M. Angelopoulos, *Synth. Met.* **1997**, *85*, 1197.
[63] Y. Yang, Q. Pei, A. J. Heeger, *J. Appl. Phys.* **1996**, *79*, 934.
[64] A. Elschner, F. Bruder, H. W. Heuer, F. Jonas, A. Karbach, S. Kirchmeyer, S. Thurm, *Synth. Met.* **2000**, *111*, 139.
[65] G. Greczynski, T. Kugler, M. Keil, W. Osikowicz, M. Fahlman, W. R. Salaneck, *J. Electron Spectrosc. Relat. Phenom.* **2003**, *121*, 1.
[66] G. Greczynski, T. Kugler, W. R. Salaneck, *Thin Solid Films* **1999**, *354*, 129.
[67] S. K. M. Jönsson, J. Birgerson, X. Crispin, G. Greczynski, W. Osikowicz, A. W. Denier van der Gon, W. R. Salaneck, M. Fahlman, *Synth. Met.* **2003**, *139*, 1.
[68] G. Zotti, S. Zecchin, G. Schiavon, F. Louwet, L. Groenendaal, X. Crispin, W. Osikowicz, W. R. Salaneck, M. Fahlman, *Macromolecules* **2003**, *36*, 3337.
[69] P. C. Jukes, S. J. Martin, A. M. Higgins, M. Geoghegan, R. A. L. Jones, S. Langridge, A. Wehrum, S. Kirchmeyer, *Adv. Mater.* **2004**, *16*, 807.
[70] See data sheets, H. C. Starck GmbH & Co. KG, Leverkusen; www.hcstarck.de, **2007**.
[71] N. Koch, A. Vollmer, A. Elschner, *Appl. Phys. Lett.* **2007**, *90*, 043512.
[72] N. Koch, A. Elschner, J. P. Rabe, R. L. Johnson, *Adv. Mater.* **2005**, *17*, 330.
[73] N. Koch, A. Vollmer, *Appl. Phys. Lett.* **2006**, *89*, 162107.
[74] C. Tengstedt, W. Osikowicz, W. R. Salaneck, I. D. Parker, C. H. Hsu, M. Fahlman, *Appl. Phys. Lett.* **2006**, *88*, 053502.
[75] A. Crispin, X. Crispin, M. Fahlman, M. Berggren, W. R. Salaneck, *Appl. Phys. Lett.* **2006**, *89*, 213503.
[76] P. J. Brewer, P. A. Lane, J. Huang, A. J. deMello, D. D. C. Bradley, J. C. deMello, *Phys. Rev. B* **2005**, *71*, 205209.
[77] D. Poplavskyy, J. Nelson, D. D. C. Bradley, *Appl. Phys. Lett.* **2003**, *83*, 707.
[78] A. J. A. B. Seeley, R. H. Friend, J. S. Kim, J. H. Burroughes, *J. Appl. Phys.* **2004**, *96*, 7643.
[79] N. Koch, A. Elschner, R. L. Johnson, *J. Appl. Phys.* **2006**, *100*, 024512.
[80] N. Koch, A. Pogantsch, E. J. W. List, G. Leising, R. I. R. Blyth, M. G. Ramsey, F. P. Netzer, *Appl. Phys. Lett.* **1999**, *74*, 2909.
[81] H. Ishii, D. Yoshimura, K. Sugiyama, S. Narioka, Y. Hamatani, I. Kawamoto, T. Miyazaki, Y. Ouchi, K. Seki, *Synth. Met.* **1997**, *85*, 1389.
[82] S. T. Lee, X. Y. Hou, M. G. Mason, C. W. Tang, *Appl. Phys. Lett.* **1998**, *72*, 1593.
[83] A. Rajagopal, A. Kahn, *J. Appl. Phys.* **1998**, *84*, 355.
[84] C. Shen, A. Kahn, J. Schwartz, *J. Appl. Phys.* **2001**, *89*, 449.
[85] C. F. Shen, I. G. Hill, A. Kahn, J. Schwartz, *J. Am. Chem. Soc.* **2000**, *122*, 5391.
[86] F. Baier, F. von Ludowig, A. Soukopp, C. Vaterlein, J. Laubender, P. Bauerle, M. Sokolowski, E. Umbach, *Opt. Mater.* **1999**, *12*, 285.
[87] R. Schlaf, C. D. Merritt, L. C. Picciolo, Z. H. Kafafi, *J. Appl. Phys.* **2001**, *90*, 1903.

[88] J. X. Tang, C. S. Lee, S. T. Lee, *Appl. Surf. Sci.* **2006**, *252*, 3948.
[89] N. Koch, L. M. Yu, V. Parente, R. Lazzaroni, R. L. Johnson, G. Leising, J. J. Pireaux, J. L. Bredas, *Adv. Mater.* **1998**, *10*, 1038.
[90] N. Koch, R. Pairleitner, Q. T. Le, E. W. Forsythe, Y. Gao, G. Leising, *Appl. Phys. Lett.* **2000**, *76*, 3738.
[91] H. Oji, E. Ito, M. Furuta, K. Kajikawa, H. Ishii, Y. Ouchi, K. Seki, *J. Electron Spectrosc. Relat. Phenom.* **1999**, *103*, 517.
[92] W. R. Salaneck, R. H. Friend, J. L. Bredas, *Phys. Rep.* **1999**, *319*, 231.
[93] N. Koch, A. Rajagopal, J. Ghijsen, R. L. Johnson, G. Leising, J. J. Pireaux, *J. Phys. Chem. B* **2000**, *104*, 1434.
[94] N. Koch, A. Rajagopal, E. Zojer, J. Ghijsen, X. Crispin, G. Pourtois, J. L. Bredas, R. L. Johnson, J. J. Pireaux, G. Leising, *Surf. Sci.* **2000**, *454–456*, 1000.
[95] M. Logdlund, P. Dannetun, S. Stafstrom, W. R. Salaneck, M. G. Ramsey, C. W. Spangler, C. Fredriksson, J. L. Bredas, *Phys. Rev. Lett.* **1993**, *70*, 970.
[96] M. Logdlund, P. Dannetun, C. Fredriksson, W. R. Salaneck, J. L. Bredas, *Phys. Rev. B* **1996**, *53*, 16327.
[97] M. G. Ramsey, D. Steinmuller, F. P. Netzer, *Phys. Rev. B* **1990**, *42*, 5902.
[98] M. G. Ramsey, M. Schatzmayr, G. Leising, F. P. Netzer, *Mol. Cryst. Liq. Cryst. Sci. Technol. Sect. A* **1994**, *256*, 679.
[99] M. Fahlman, D. Beljonne, M. Logdlund, R. H. Friend, A. B. Holmes, J. L. Bredas, W. R. Salaneck, *Chem. Phys. Lett.* **1993**, *214*, 327.
[100] G. Greczynski, M. Fahlman, W. R. Salaneck, N. Johansson, D. A. dos Santos, A. Dkhissi, J. L. Brédas, *J. Chem. Phys.* **2002**, *116*, 1700.
[101] M. Schamberg, J. Hu, J. Kanzow, K. Rätzke, R. Adelung, F. Faupel, C. Pannemann, U. Hilleringmann, S. Meyer, J. Pflaum, *Appl. Phys. Lett.* **2005**, *86*, 024104.
[102] A. C. Dürr, N. Koch, M. Kelsch, A. Rühm, J. Ghijsen, R. L. Johnson, J.-J. Pireaux, J. Schwartz, F. Schreiber, H. Dosch, A. Kahn, *Phys. Rev. B* **2003**, *68*, 115428.
[103] N. Koch, C. Chan, J. Schwartz, A. Kahn, *Phys. Rev. B* **2003**, *67*, 195330.
[104] D. Yoshimura, T. Yokoyama, E. Ito, H. Ishii, Y. Ouchi, S. Hasegawa, K. Seki, *Synth. Met.* **1999**, *102*, 1145.
[105] Q.-T. Le, L. Yan, Y. G. Gao, M. G. Mason, D. J. Giesen, C. W. Tang, *J. Appl. Phys.* **2000**, *87*, 375.
[106] M. G. Mason, C. W. Tang, L. S. Hung, P. Raychaudhuri, J. Madathil, D. J. Giesen, L. Yan, Q. T. Le, Y. Gao, S. T. Lee, L. S. Liao, L. F. Cheng, W. R. Salaneck, D. A. dos Santos, J. L. Bredas, *J. Appl. Phys.* **2001**, *89*, 2756.
[107] G. Greczynski, M. Fahlman, W. R. Salaneck, *Appl. Surf. Sci.* **2000**, *166*, 380.
[108] G. Greczynski, W. R. Salaneck, M. Fahlman, *Appl. Surf. Sci.* **2001**, *175*, 319.
[109] E. J. W. List, J. Partee, J. Shinar, U. Scherf, K. Müllen, E. Zojer, K. Petritsch, G. Leising, W. Graupner, *Phys. Rev. B* **2000**, *61*, 10807.
[110] U. Scherf, E. J. W. List, *Adv. Mater.* **2002**, *14*, 477.
[111] O. D. Jurchescu, J. Baas, T. T. M. Palstra, *Appl. Phys. Lett.* **2005**, *87*, 052102.
[112] J. Blochwitz, M. Pfeiffer, T. Fritz, K. Leo, *Appl. Phys. Lett.* **1998**, *73*, 729.
[113] M. Pfeiffer, A. Beyer, T. Fritz, K. Leo, *Appl. Phys. Lett.* **1998**, *73*, 3202.
[114] W. Y. Gao, A. Kahn, *Appl. Phys. Lett.* **2001**, *79*, 4040.
[115] B. Maennig, M. Pfeiffer, A. Nollau, X. Zhou, K. Leo, P. Simon, *Phys. Rev. B* **2001**, *64*, 195208.
[116] W. Y. Gao, A. Kahn, *J. Appl. Phys.* **2003**, *94*, 359.
[117] W. Y. Gao, A. Kahn, *J. Phys. Condens. Matter* **2003**, *15*, S2757 – S2770.
[118] W. Y. Gao, A. Kahn, *Org. Electron.* **2002**, *3*, 53.
[119] A. Nollau, M. Pfeiffer, T. Fritz, K. Leo, *J. Appl. Phys.* **2000**, *87*, 4340.
[120] A. G. Werner, F. Li, K. Harada, M. Pfeiffer, T. Fritz, K. Leo, *Appl. Phys. Lett.* **2003**, *82*, 4495.
[121] C. K. Chan, E. G. Kim, J. L. Bredas, A. Kahn, *Adv. Funct. Mater.* **2006**, *16*, 831.
[122] C. K. Chan, F. Amy, Q. Zhang, S. Barlow, S. Marder, A. Kahn, *Chem. Phys. Lett.* **2006**, *431*, 67.
[123] N. Koch, G. Leising, L. M. Yu, A. Rajagopal, J. J. Pireaux, R. L. Johnson, *J. Vac. Sci. Technol. A* **2000**, *18*, 295.
[124] T. Matsushima, C. Adachi, *Appl. Phys. Lett.* **2006**, *89*, 253506.
[125] M. Pfeiffer, S. R. Forrest, X. Zhou, K. Leo, *Org. Electron.* **2003**, *4*, 21.
[126] M. Pfeiffer, S. R. Forrest, K. Leo, M. E. Thompson, *Adv. Mater.* **2002**, *14*, 1633.
[127] R. Meerheim, K. Walzer, M. Pfeiffer, K. Leo, *Appl. Phys. Lett.* **2006**, *89*, 06111.
[128] M. A. Baldo, D. F. O'Brien, Y. You, A. Shoustikov, S. Sibley, M. E. Thompson, S. R. Forrest, *Nature* **1998**, *395*, 151.
[129] J. W. Verhoeven, *Pure Appl. Chem.* **1996**, *68*, 2223.
[130] J. M. Lupton, A. Pogantsch, T. Piok, E. J. W. List, S. Patil, U. Scherf, *Phys. Rev. Lett.* **2002**, *89*, 167401.
[131] Y. Sun, N. C. Giebink, H. Kanno, B. Ma, M. E. Thompson, S. R. Forrest, *Nature* **2006**, *440*, 908.
[132] G. Schwartz, K. Fehse, M. Pfeiffer, K. Walzer, K. Leo, *Appl. Phys. Lett.* **2006**, *89*, 083509.
[133] X. Z. Jiang, A. K. Y. Jen, B. Carlson, L. R. Dalton, *Appl. Phys. Lett.* **2002**, *81*, 3125.
[134] C. D. Müller, T. Braig, H. G. Nothofer, M. Arnoldi, M. Gross, U. Scherf, O. Nugken, K. Meerholz, *ChemPhysChem* **2000**, *1*, 207.
[135] C. D. Müller, A. Falcou, N. Reckefuss, M. Rojahn, V. Wiederhirn, P. Rudati, H. Frohne, O. Nuyken, K. Meerholz, *Nature* **2003**, *421*, 829.
[136] H. Yan, Q. Huang, B. J. Scott, T. J. Marks, *Appl. Phys. Lett.* **2004**, *84*, 3873.
[137] X. Yang, D. C. Müller, D. Neher, K. Meerholz, *Adv. Mater.* **2006**, *18*, 948.
[138] S. Setayesh, A. C. Grimsdale, T. Weil, V. Enkelmann, K. Müllen, F. Meghdadi, E. J. W. List, G. Leising, *J. Am. Chem. Soc.* **2001**, *123*, 946.
[139] W. K. Huang, W. S. Wang, H. C. Kan, F. C. Chen, *Jpn. J. Appl. Phys. Part 1* **2006**, *45*, L1100.
[140] Y. Sun, S. R. Forrest, *J. Appl. Phys.* **2006**, *100*, 073106.
[141] G. A. Chamberlain, *Solar Cells* **1983**, *8*, 47.
[142] C. W. Tang, A. C. Albrecht, *J. Chem. Phys.* **1975**, *62*, 2139.
[143] R. N. Marks, J. J. M. Halls, D. D. C. Bradley, R. H. Friend, A. B. Holmes, *J. Phys. Condens. Matter* **1994**, *6*, 1379.
[144] C. W. Tang, *Appl. Phys. Lett.* **1986**, *48*, 183.
[145] http://rredc.nrel.gov/solar/spectra/am1.5 **2007**.
[146] E. Perzon, X. Wang, F. Zhang, W. Mammo, J. L. Delgado, P. de La Cruz, O. Inganäs, F. Langa, M. R. Andersson, *Synth. Met.* **2005**, *154*, 53.
[147] M. Svensson, F. Zhang, S. C. Veenstra, W. J. H. Verhees, J. C. Hummelen, J. M. Kroon, O. Inganas, M. R. Andersson, *Adv. Mater.* **2003**, *15*, 988.
[148] E. Zojer, N. Koch, P. Puschnig, F. Meghdadi, A. Niko, R. Resel, C. Ambrosch-Draxl, M. Knupfer, J. Fink, J. L. Bredas, G. Leising, *Phys. Rev. B* **2000**, *61*, 16538.
[149] V. Bulovic, S. R. Forrest, *Chem. Phys. Lett.* **1995**, *238*, 88.
[150] M. Granström, K. Petritsch, A. C. Arias, A. Lux, M. R. Andersson, R. H. Friend, *Nature* **1998**, *395*, 257.
[151] J. J. Halls, C. A. Walsh, N. C. Greenham, E. A. Marseglia, R. H. Friend, S. C. Moratti, A. B. Holmes, *Nature* **1995**, *376*, 498.
[152] G. Yu, A. J. Heeger, *J. Appl. Phys.* **1995**, *78*, 4510.
[153] G. Yu, J. Gao, J. C. Hummelen, F. Wudl, A. J. Heeger, *Science* **1995**, *270*, 1789.
[154] L. Schmidt-Mende, A. Fechtenkötter, K. Müllen, E. Moons, R. H. Friend, J. D. MacKenzie, *Science* **2001**, *293*, 1119.
[155] W. Ma, C. Yang, X. Gong, K. Lee, A. J. Heeger, *Adv. Funct. Mater.* **2005**, *15*, 1617.
[156] P. Peumans, S. Uchida, S. R. Forrest, *Nature* **2003**, *425*, 158.
[157] S. Sellner, A. Gerlach, F. Schreiber, M. Kelsch, N. Kasper, H. Dosch, S. Meyer, J. Pflaum, M. Fischer, B. Gompf, *Adv. Mater.* **2004**, *16*, 1750.
[158] K. Robbie, M. J. Brett, A. Lakhtakia, *Nature* **1996**, *384*, 616.
[159] P. C. P. Hrudey, K. L. Westra, M. J. Brett, *Adv. Mater.* **2006**, *18*, 224.
[160] J. Zhang, I. Salzmann, F. Zhang, Z. Xu, S. Rogaschewski, J. P. Rabe, N. Koch, *Appl. Phys. Lett.* **2007**, *90*, 193117.
[161] N. S. Sariciftci, L. Smilowitz, A. J. Heeger, F. Wudl, *Science* **1992**, *258*, 1474.
[162] H. Hoppe, N. S. Sariciftci, *J. Mater. Chem.* **2006**, *16*, 45.
[163] I. G. Hill, A. Kahn, *J. Appl. Phys.* **1998**, *84*, 5583.
[164] A. Rajagopal, N. Koch, J. Ghijsen, K. Kaeriyama, R. L. Johnson, G. Leising, J.-J. Pireaux, *Met. Plast.* **2001**, *7*, 1.
[165] A. Rajagopal, A. Kahn, *Adv. Mater.* **1998**, *10*, 140.
[166] W. Y. Gao, A. Kahn, *Appl. Phys. Lett.* **2003**, *82*, 4815.
[167] N. Koch, I. Salzmann, R. L. Johnson, J. Pflaum, R. Friedlein, J. P. Rabe, *Org. Electron.* **2006**, *7*, 537.
[168] A. Kahn, W. Zhao, W. Gao, H. Vazquez, F. Flores, *Chem. Phys.* **2006**, *325*, 129.
[169] A. C. Morteani, P. Sreearunothai, L. M. Herz, R. H. Friend, C. Silva, *Phys. Rev. Lett.* **2004**, *92*, 247402.
[170] A. Zen, J. Pflaum, S. Hirschmann, W. Zhuang, F. Jaiser, U. Asawapirom, J. P. Rabe, U. Scherf, D. Neher, *Adv. Funct. Mater.* **2004**, *14*, 757.

[171] G. Horowitz, R. Hajlaoui, F. Kouki, *Eur. Phys. J. Appl. Phys.* **1998**, *1*, 361.
[172] M. Zhu, G. Liang, T. Cui, K. Varahramyan, *Solid State Electron.* **2003**, *47*, 1855.
[173] G. Horowitz, R. Hajlaoui, H. Bouchriha, R. Bourguiga, M. Hajlaoui, *Adv. Mater.* **1998**, *10*, 923.
[174] C. R. Newman, C. D. Frisbie, D. A. da Silva Filho, J. L. Bredas, P. C. Ewbank, K. R. Mann, *Chem. Mater.* **2004**, *16*, 4436.
[175] Naraso, J. Nishida, D. Kumaki, S. Tokito, Y. Yamashita, *J. Am. Chem. Soc.* **2006**, *128*, 9598.
[176] L. L. Chua, J. Zaumseil, J. F. Chang, E. C. W. Ou, P. K. H. Ho, H. Sirringhaus, R. H. Friend, *Nature* **2005**, *434*, 194.
[177] T. B. Singh, F. Meghdadi, S. Gunes, N. Marjanovic, G. Horowitz, P. Lang, S. Bauer, N. S. Sariciftci, *Adv. Mater.* **2005**, *17*, 2315.
[178] M.-H. Yoon, C. Kim, A. Facchetti, T. J. Marks, *J. Am. Chem. Soc.* **2006**, *128*, 12851.
[179] J. M. Kim, J. W. Lee, J. K. Kim, B. K. Ju, J. S. Kim, Y. H. Lee, M. H. Oh, *Appl. Phys. Lett.* **2004**, *85*, 6368.
[180] S. Kobayashi, T. Nishikawa, T. Takenobu, S. Mori, T. Shimoda, T. Mitani, H. Shimotani, N. Yoshimoto, S. Ogawa, Y. Iwasa, *Nat. Mater.* **2004**, *3*, 317.
[181] M. McDowell, I. G. Hill, J. E. McDermott, S. L. Bernasek, J. Schwartz, *Appl. Phys. Lett.* **2006**, *88*, 073505.
[182] T. W. Kelley, P. F. Baude, C. Gerlach, D. E. Ender, D. Muyres, M. A. Haase, D. E. Vogel, S. D. Theiss, *Chem. Mater.* **2004**, *16*, 4413.
[183] S. Lee, B. Koo, J. Shin, E. Lee, H. Park, H. Kim, *Appl. Phys. Lett.* **2006**, *88*, 162109.
[184] O. D. Jurchescu, J. Baas, T. T. M. Palstra, *Appl. Phys. Lett.* **2004**, *84*, 3061.
[185] M. Pope, C. E. Swenberg, *Electronic Processes in Organic Crystals and Polymers*, Oxford University Press, Oxford, **1999**.
[186] R. Ruiz, B. Nickel, N. Koch, L. C. Feldman, R. F. Haglund, A. Kahn, G. Scoles, *Phys. Rev. B* **2003**, *67*, 125406.
[187] F. Schreiber, *Phys. Status Solidi A* **2004**, *201*, 1037.
[188] G. Witte, C. Wöll, *J. Mater. Res.* **2004**, *19*, 1889.
[189] F. Dinelli, M. Murgia, P. Levy, M. Cavallini, F. Biscarini, *Phys. Rev. Lett.* **2004**, *92*, 116802.
[190] K. Puntambekar, J. Dong, G. Haugstad, C. D. Frisbie, *Adv. Funct. Mater.* **2006**, *16*, 879.
[191] B. Stadlober, U. Haas, H. Maresch, A. Haase, *Phys. Rev. B* **2006**, *74*, 165302.
[192] J. H. Kang, D. A. da Silva Filho, J. L. Bredas, X. Y. Zhu, *Appl. Phys. Lett.* **2005**, *86*, 152115.
[193] V. Ignatescu, J. C. M. Hsu, A. C. Mayer, J. M. Blakely, G. G. Malliaras, *Appl. Phys. Lett.* **2006**, *89*, 253116.
[194] S. Steudel, S. D. Vusser, K. Myny, M. Lenes, J. Genoe, P. Heremans, *J. Appl. Phys.* **2002**, *99*, 114519.
[195] C. D. Dimitrakopoulos, P. R. L. Malenfant, *Adv. Mater.* **2002**, *14*, 99.
[196] J. N. Haddock, X. Zhang, S. Zheng, Q. Zhang, S. R. Marder, B. Kippelen, *Org. Electron.* **2006**, *7*, 45.
[197] K. Tsukagoshi, I. Yagi, K. Shigeto, K. Yanagisawa, J. Tanabe, Y. Aoyagi, *Appl. Phys. Lett.* **2005**, *87*, 183502.
[198] B. Stadlober, U. Haas, H. Gold, A. Haase, G. Leising, N. Koch, S. Rentenberger, E. Zojer, unpublished results.
[199] M. Maccioni, E. Orgiu, P. Cosseddu, S. Locci, A. Bonfiglio, *Appl. Phys. Lett.* **2006**, *89*, 143515.
[200] A. Hepp, H. Heil, W. Weise, M. Ahles, R. Schmechel, H. von Seggern, *Phys. Rev. Lett.* **2003**, *91*, 157406.
[201] K. Kudo, *Curr. Appl. Phys.* **2005**, *5*, 337.
[202] M. Muccini, *Nat. Mater.* **2006**, *5*, 605.
[203] S. Möller, C. Perlov, W. Jackson, C. Taussig, S. R. Forrest, *Nature* **2003**, *426*, 166.
[204] L. P. Ma, J. Liu, Y. Yang, *Appl. Phys. Lett.* **2002**, *80*, 2997.
[205] L. Ma, S. Pyo, J. Ouyang, Q. Xu, Y. Yang, *Appl. Phys. Lett.* **2003**, *82*, 1419.
[206] N. Koch, A. C. Dürr, J. Ghijsen, R. L. Johnson, J.-J. Pireaux, J. Schwartz, F. Schreiber, H. Dosch, A. Kahn, *Thin Solid Films* **2003**, *441*, 145.
[207] Y. Yang, J. Ouyang, L. P. Ma, R. J. H. Tseng, C. W. Chu, *Adv. Funct. Mater.* **2006**, *16*, 1001.

Received: March 8, 2007
Published online on May 31, 2007

